# The method of time-ordered graph decoupling and its application to the description of giant resonances in magic nuclei

S. P. Kamerdzhiev and G. Ya. Tertychnyĭ
*State Scientific Center of the Russian Federation, Physics and Power Engineering Institute, Obninsk*

V. I. Tselyaev
*Physics Institute, St. Petersburg State University*

Fiz. Élem. Chastits At. Yadra **28**, 333–390 (March–April 1997)

A microscopic approach to analyzing the excited states of magic nuclei is described. It is based on the systematic use of the method of quantum Green functions. When applied to the theory of giant multipole resonances, the approach explicitly includes the three principle mechanisms of resonance formation in a finite nucleus: decay via particle–hole configurations of the discrete spectrum, decay via particle–hole configurations with a particle in the continuum, and decay via more complicated configurations of the particle–hole⊗phonon type. The results of a numerical realization of this approach for describing giant resonances in magic stable and unstable nuclei are discussed. © *1997 American Institute of Physics.* [S1063-7796(97)00202-7]

## 1. INTRODUCTION

In the microscopic theory of nuclear structure at low excitation energies[1)] it has become almost axiomatic that the random-phase approximation (RPA) must be improved by including configurations more complex than the particle–hole ($1p1h$) ones included in the RPA. This statment rests on the fact that it has proved impossible to explain the total widths of giant multipole resonances (GMRs) using the RPA (see, for example, Refs. 1–3). It is well known that the GMR widths have three formation mechanisms: (1) an analog of Landau damping, determined by the distribution of the transition strength among discrete RPA states; (2) decay of an excited state into the continuum, where the one-particle continuum apparently plays the leading role (it forms the width $\Gamma\uparrow$); (3) additional resonance fragmentation due to the coupling of RPA configurations to more complex ones, primarily $2p2h$ configurations (this forms the width $\Gamma\downarrow$). Numerous estimates of the effect of $2p2h$ configurations (see, for example, Ref. 3), confirmed by more accurate calculations (to be discussed below), have shown that this effect gives the dominant contribution to the width $\Gamma\downarrow$ for intermediate and heavy nuclei.

Until recently, the microscopic theory of GMRs has developed in two different directions: RPA+continuum and RPA+$2p2h$. The first problem can now be considered solved, at least for an effective contact interaction between nucleons; the use of the Green function method has made it possible to include the one-particle continuum exactly by transforming to the coordinate representation in the RPA equations.[4,5] Other methods for solving this problem have also been developed which admit the use of nonlocal forces (see, for example, Refs. 6 and 7). As far as the problem of including $2p2h$ configurations is concerned, by now it is quite obvious that the approaches to solving it are considerably more diverse in both the technique used and the physical content than those for the inclusion of $1p1h$ configurations.

The discovery of new GMRs in 1971–1972 strongly stimulated the development of the theory, including approaches for including complex configurations. Already by that time the quasiparticle–phonon model[8] was the best method of calculating this effect, and a method of including two-phonon configurations in intermediate and heavy nuclei was systematically developed for this model. Later on, methods were developed for including "pure" $2p2h$ configurations [examples are the second RPA (SRPA), Ref. 9, and the extended SRPA (ESRPA), Refs. 2, 10, and 11], along with methods based on the use of RPA collectivization, as a rule, in one of the two $1p1h$ channels, i.e., models including $1p1h$⊗phonon configurations. This latter category includes methods[12,13] based on nuclear field theory and the Bohr–Mottelson strength-function model, models developed within the Green function formalism,[14–18] and several others (here we cite only the basic approaches which will be discussed below; see the literature cited in Refs. [1–3, 14, 15, and 17] for more detail).

The current trends in the experimental physics of GMRs sustain the interest in developing the microscopic theory, and in some sense they can be viewed as a challenge to the theory. Here we have in mind, first, the significant improvement in the experimental resolution to $\Delta E \simeq 10$ keV and better, which has already generated and will continue to generate data on the GMR fine structure, not to mention the other information already obtained.[19–22] Second, at present special attention is being paid to the study of unstable nuclei, which are of great interest in nuclear physics and astrophysics, and studies are being performed using radioactive beams. From the viewpoint of the microscopic nuclear theory, the first trend implies the need for the simultaneous inclusion of the continuum and complex configurations in addition to the discrete RPA ones, while the second implies that the theory, whose parameters are already known, must be applicable to nuclei which have not been studied experimentally. It turns out that a theory satisfying all these requirements is very difficult to realize numerically. Only quite recently have all three mechanisms of GMR decay been included simulta-

 1063-7796/97/020134-25$10.00  

neously (Refs. 17 and 23–27), of course, using very different approximations and methods, and for various magic nuclei and resonances. Most of the calculations of this type have been performed using the approach discussed in the present review, based on the Green function method (Refs. 17 and 27–34.

Regarding practical applications, this approach can be viewed as a further development of the ideas of the theory of finite Fermi systems (TFFS),[35] the parameters of which have turned out to be fairly universal for all nuclei except light ones. Whereas in the traditional treatment the theory of finite Fermi systems is the RPA formulated in terms of the Green function method, the problem of the explicit inclusion of configurations more complex than those in the RPA is solved in this new approach. We shall mainly study $1p1h\otimes$phonon configurations. This is because the problem of including "pure" $2p2h$ configurations involves not only quantitative difficulties, but also has the drawback of not having any real small parameter. It is preferable, at least at present, to use basis configurations in which the collectivization in one or both $1p1h$ channels is already included, i.e., configurations of the type $1p1h\otimes$phonon or phonon$\otimes$phonon.[8] In this case the small parameter is the dimensionless squared quasiparticle–phonon interaction amplitude: $g^2<1$ (Refs. 43 and 14). This greatly simplifies the problem of including $2p2h$ or, more precisely, $1p1h\otimes$phonon configurations, because:

1. We obtain a general principle for selecting terms. It becomes possible to keep only terms through second order in $g$ (however, this is not valid for all the quantities involved in the theory; this question will be discussed in this review).

2. Moreover, we can limit ourselves to the inclusion of only $1p1h\otimes$phonon configurations containing collective phonons with the maximum value of $g^2$. Since the most important contribution near the GMR energy comes from low-lying phonons, it is reasonable to restrict ourselves to low-lying collective phonons, of which there are not many. The other phonons are effectively included via the phenomenological parameters of the problem.

3. The restriction to a small number of collective phonons is especially important if one uses phenomenological local forces with parameters selected within the framework of the theory of finite Fermi systems. These parameters should not change greatly when the additional nonlocal long-range forces arising from the inclusion of a small number of collective phonons in $1p1h\otimes$phonon configurations are included. Therefore, in this case it is possible, at least in a first approximation, to leave the TFFS parameters unchanged. Our calculations have confirmed the validity of this approximation. In addition, the restriction to a small number of phonons noticeably eases the numerical difficulties, which is very important for problems with nonseparable interaction.

An approach to the inclusion of $1p1h\otimes$phonon configurations using the Green function method has been developed in Refs. 14 and 16 on the basis of these ideas. Its numerical realization for $M1$ resonances in magic nuclei has produced quite reasonable results. In particular, it has been shown that the observed $M1$ excitations in $^{40}$Ca with energy $\sim 10$ MeV and in $^{16}$O with energy $\sim 16$ MeV are explained by correlations in the ground state due only to $1p1h\otimes$phonon configurations (the RPA does not give a $1^+$ level in this region).[16] This was an important result which demonstrated the role of these effects and suggested that they could be analyzed systematically within the framework of the Green function method.

However, the further application of the approach of Refs. 14 and 16 was complicated by the appearance of the "problem of second-order poles," which will be described in Sec. IV below. This problem was later formally eliminated in the model of Ref. 15, but the solution of the equations of that model proved to be very difficult for real nuclei.

This review is devoted to describing the new approach, developed on the basis of the Green function formalism, to the problem of including complex configurations. It allows the construction of various classes of models: ones taking into account "pure" $2p2h$ configurations (like the SRPA) and ones taking into account $1p1h\otimes$phonon configurations. The main element of this approach, which effects the passage from general exact equations to a specific solvable model, is the method of constructing the generalized particle–hole propagator.[18] The physical meaning of the approximations used in this method is closely related to the Feynman-diagram interpretation of the quantities entering into the theory.[35] In the model including $1p1h\otimes$phonon configurations, the propagator[18] contains a class of graphs which is wider than in Refs. 14 and 16 but narrower than in Ref. 15. The partial summation of the diagrammatic series in the propagator of Ref. 18 solved the problem of second-order poles mentioned above. The first calculations performed using this approach and neglecting the contribution of the one-particle continuum[18,36] in many respects were a repetition of the earlier calculations,[16] but, in contrast to Ref. 16, they led to a unified description of both the isovector and the isoscalar part of the $M1$-strength distribution in $^{208}$Pb. The results of using this approach to describe other GMRs including the continuum in $1p1h\otimes$phonon configurations[17,27–34] will be discussed in Sec. 6.

One of the advantages of the Green function method is that, being a consistent many-body theory, it contains many general and exact relations between the quantities involved in its technical apparatus. The most typical examples of such relations which we use are the Dyson equation for the one-particle Green function and the equation for the response function. By using the physical and mathematical properties of these quantities and the corresponding physical approximations, the leading one of which is the explicit isolation of complex configurations of a certain class, i.e., $1p1h\otimes$phonon configurations containing collective phonons, we transform the corresponding relations into equations which can be analyzed and solved by computer. In this special type of deductive approach, the correct choice of the initial approximations and input parameters of the problem becomes very important. Monitoring these by model-independent and limiting expressions of the theory proves to be very useful, as does the presence of a small parameter. In our opinion, this type of approach allows a sufficiently complete understanding of the physics of the problem and the uniform inclusion of the main features of the phenomenon

under study. This is especially important for a problem as complicated as the inclusion of $2p2h\otimes$phonon or $1p1h\otimes$phonon configurations in a finite nucleus.

This review has 7 sections. In Sec. 2 we give the basics of the Green function method as applied to the inclusion of complex configurations. In Sec. 3 we study the technical details of the construction of the generalized particle–hole propagator. Section 4 is devoted to the derivation of the equations determining this propagator in our approach. In Sec. 5 we discuss the properties of the propagator, briefly consider models for the inclusion of "pure" $2p2h$ configurations, and describe the effects of ground-state correlations due to $1p1h\otimes$phonon configurations. In Sec. 6 we discuss a method, useful for further applications, of including the one-particle continuum in the equation for the variation of the density matrix, and we present the results of calculations performed using our model including $1p1h\otimes$phonon configurations with Landau–Migdal effective forces. The discussion of the numerical results is fairly brief and intended only as an illustration. In the conclusion (Sec. 7) we summarize the main results and list possible ways of improving and extending the methods of including the three main mechanisms of GMR formation.

## 2. THEORETICAL FOUNDATIONS OF THE DESCRIPTION OF NUCLEAR EXCITATIONS IN THE GREEN FUNCTION METHOD

### 2.1. General relations

The solution of the problem of describing the excitation spectrum of an even–even nucleus, including giant resonances, can in many interesting cases be reduced to the calculation of the function describing the distribution of the strengths of transitions in the nucleus induced by an external field $V^0$ (the strength function):

$$S(E)=\sum_{n\neq 0}\left(|\langle n|V^{0+}|0\rangle|^2\delta(E-\omega_n)\right.$$
$$\left.-|\langle n|V^0|0\rangle|^2\delta(E+\omega_n)\right),$$

where $\omega_n=E_n-E_0$, and $E_n$ and $|n\rangle$ are the exact eigenenergy and eigenfunction of the initial nuclear Hamiltonian, which characterize a state with a set of quantum numbers denoted by $n$ ($n=0$ corresponds to the ground state). In the Green function method the strength function is completely determined by the response function of the nucleus $R(\omega)$, because it follows from the spectral expansion of the response function that[2)]

$$S(E)=\frac{1}{\pi}\lim_{\Delta\to+0}\operatorname{Im}\sum_{1234}V^{0*}_{21}R_{12,34}(E+i\Delta)V^0_{43}. \tag{1}$$

Formally, the response function is the solution of the Bethe–Salpeter equation in the particle–hole ($p-h$) channel:

$$R_{12,34}(\omega)=\int_{-\infty}^{\infty}\frac{d\varepsilon}{2\pi i}R_{12,34}(\omega,\varepsilon), \tag{2}$$

$$R_{12,34}(\omega,\varepsilon)=-G_{31}(\varepsilon+\omega)G_{24}(\varepsilon)$$
$$+\sum_{5678}G_{51}(\varepsilon+\omega)G_{26}(\varepsilon)\int_{-\infty}^{\infty}\frac{d\varepsilon'}{2\pi i}$$
$$\times\mathcal{V}_{56,78}(\omega,\varepsilon,\varepsilon')R_{78,34}(\omega,\varepsilon'), \tag{3}$$

where $G$ is the exact one-particle Green function, and $\mathcal{V}$ is the amplitude of the nucleon–nucleon interaction in a nuclear medium, which is irreducible in the $p-h$ channel. However, (3) is actually only one of the equations entering into the closed system of nonlinear functional differential equations, the solution of which corresponds to the exact solution of the many-body problem and determines both the function $R$ and other quantities in the many-body theory[35] (the formulation of this system, generalized to include many-nucleon interactions, is given in Ref. 37). In particular, this system of equations includes the relation (in the time representation, $1=\{1,t_1\}$ and so on)

$$\mathcal{V}(12,34)=i\frac{\delta\Sigma(3,4)}{\delta G(1,2)}, \tag{4}$$

where $\Sigma$ is the one-particle mass operator related to the Green function $G$ by the Dyson equation:

$$G_{12}(\varepsilon)=G^0_{12}(\varepsilon)+\sum_{34}G^0_{13}(\varepsilon)\Sigma_{34}(\varepsilon)G_{42}(\varepsilon), \tag{5}$$

in which $G^0_{12}(\varepsilon)=((\varepsilon-\mathbf{p}^2/2m)^{-1})_{12}$ is the free Green function.

The above discussion implies that Eq. (3) can be viewed as the definition of the response function $R$ only when the quantities $\Sigma$ and $\mathcal{V}$ are known. In fact, we have at our disposal only model approximations of these quantities. The simplest and clearest algorithm for constructing these approximations is that of rearranged perturbation theory in the vacuum internucleon interaction $w$ (in the final expressions this is replaced by the effective interaction in the medium), which in practice reduces to the iterative solution of the system of functional differential equations.[37] The rearrangement of perturbation theory amounts to the following. Instead of the free Green function $G^0$ we introduce a new "bare" Green function $\widetilde{G}$ which is the solution of the Dyson equation

$$\widetilde{G}_{12}(\varepsilon)=G^0_{12}(\varepsilon)+\sum_{34}G^0_{13}(\varepsilon)\widetilde{\Sigma}_{34}\widetilde{G}_{42}(\varepsilon) \tag{6}$$

with as yet undetermined mass operator $\widetilde{\Sigma}$. It is only assumed that the latter is independent of the energy variable. After this, Eq. (5) is transformed into the rearranged Dyson equation

$$G_{12}(\varepsilon)=\widetilde{G}_{12}(\varepsilon)+\sum_{34}\widetilde{G}_{13}(\varepsilon)\Sigma^e_{34}(\varepsilon)G_{42}(\varepsilon), \tag{7}$$

in which the mass operator $\Sigma^e$ is given by

$$\Sigma_{12}(\varepsilon)=\widetilde{\Sigma}_{12}+\Sigma^e_{12}(\varepsilon), \tag{8}$$

which follows from the condition that the solutions of (5)

and (7) coincide. The function $\tilde{G}$ specifies a "point," more convenient than $G^0$, about which the perturbation series for $G$ and other quantities are constructed.[3)] Isolation of the reference term $\tilde{\Sigma}$ from the complete mass operator $\Sigma$ leads to isolation of the analogous term $\tilde{\mathcal{U}}$, independent of the energy variables, from the amplitude $\mathcal{U}$:

$$\mathcal{U}_{12,34}(\omega,\varepsilon,\varepsilon')=\tilde{\mathcal{U}}_{12,34}+\mathcal{U}^e_{12,34}(\omega,\varepsilon,\varepsilon'). \tag{9}$$

This is related to the fact that the mass operator $\Sigma$ and the amplitude $\mathcal{U}$, and, consequently, all their components, must satisfy Eq. (4) in addition to the known consistency conditions.[35] In particular, since the functions $\Sigma^e$ and $\mathcal{U}^e$ completely determine the energy dependence of $\Sigma$ and $\mathcal{U}$ (which explains the notation we have used for them), the following dynamical consistency condition must be satisfied:[38]

$$\Sigma^e_{12}(\varepsilon+\omega)-\Sigma^e_{12}(\varepsilon)=\int_{-\infty}^{\infty}\frac{d\varepsilon'}{2\pi i}\sum_{34}\mathcal{U}^e_{21,43}(\omega,\varepsilon,\varepsilon') \times[G_{34}(\varepsilon'+\omega)-G_{34}(\varepsilon')], \tag{10}$$

which follows from the particle number conservation law. All the consistency conditions, both static[35] and dynamical,[38] remain valid also when nucleon multiparticle interactions are switched on.[37]

### 2.2. Model approximations for the mass operator $\Sigma$ and the amplitude $\mathcal{U}$

Let us turn to the definition of $\tilde{\Sigma}$ and $\tilde{\mathcal{U}}$. It follows from the preceding discussion that formally they are not subject to any important constraints except the static consistency condition between them. However, from the microscopic point of view it is convenient to take, for example, $\tilde{\Sigma}$ to be the Hartree–Fock approximation for the mass operator $\Sigma$, and to define $\tilde{\mathcal{U}}$, according to (4), as $\tilde{\mathcal{U}}=i\delta\tilde{\Sigma}/\delta\tilde{G}$ (when many-nucleon interactions are included the amplitude $\tilde{\mathcal{U}}$ defined in this manner acquires a functional density dependence). This choice is convenient because then there are no contributions to the functions $\Sigma^e$ and $\mathcal{U}^e$ of first order in the interaction, so that in first-order perturbation theory we obtain $\Sigma=\tilde{\Sigma}$ and $\mathcal{U}=\tilde{\mathcal{U}}$. The definition of the mass operator $\tilde{\Sigma}$, for example, in the Hartree–Fock approximation, is essentially equivalent to choosing the basis functions of configuration space, because in this formalism this space is formed from states characterized by elements of the basis $\{\tilde{\phi}_1,\tilde{\varepsilon}_1\}$ diagonalizing the Green function $\tilde{G}$:

$$\tilde{G}_{12}(\varepsilon)=\delta_{12}\tilde{G}_1(\varepsilon),\quad \tilde{G}_1(\varepsilon)=\frac{1}{\varepsilon-\tilde{\varepsilon}_1+i\sigma_1\delta},\quad \delta\to+0. \tag{11}$$

Here we have introduced the quantity $\sigma_1$, which is equal to $+1$ for particles and $-1$ for holes and is related to the level occupation number as $\sigma_1=1-2n_1$.

Let us return to Eq. (3), which is the starting point of our approach. From Eqs. (2), (3), and (5) it follows that the approximation $\Sigma=\tilde{\Sigma}$, $\mathcal{U}=\tilde{\mathcal{U}}$ corresponds to the random-phase approximation (RPA) for the response function $R(\omega)$. And since only the $1p1h$ part of the response function is completely determined in the RPA (complex configurations are taken into account only within the RPA ground-state correlations), our problem of including more complex $(2p2h)$ configurations requires choosing the approximations of the functions $\Sigma^e$ and $\mathcal{U}^e$ and the method of solving (3) with $\Sigma$ and $\mathcal{U}$ given by Eqs. (8) and (9). In other words, it is $\Sigma^e$ and $\mathcal{U}^e$ which are responsible for the coupling of $1p1h$ configurations to more complicated ones.

Following the algorithm of rearranged perturbation theory, we find that the contribution of second order in the internucleon interaction $w$ to the functions $\Sigma^e$ and $\mathcal{U}^e$ is given by (in second order we neglect the two-particle interaction with the antisymmetrized amplitude $w_{12,34}=w^{(2)}_{12,34}$, in accordance with the notation of Refs. 37 and 39):

$$\Sigma^e_{12}(\varepsilon)=\frac{1}{2}\sum_{345}\delta_{\sigma_3,-\sigma_4}\delta_{\sigma_5-\sigma_4}\frac{w_{14,35}w_{35,24}}{\varepsilon+\tilde{\varepsilon}_4-\tilde{\varepsilon}_3-\tilde{\varepsilon}_5+i\sigma_3\delta}, \tag{12}$$

$$\mathcal{U}^e_{12,34}(\omega,\varepsilon,\varepsilon')=\sum_{56}\sigma_6\delta_{\sigma_5,-\delta_6}\frac{w_{53,16}w_{26,54}}{\varepsilon-\varepsilon'-\tilde{\varepsilon}_5+\tilde{\varepsilon}_6+i\sigma_5\delta} +\frac{1}{2}\sum_{56}\sigma_5\delta_{\sigma_5\sigma_6} \times\frac{w_{23,56}w_{56,14}}{\omega+\varepsilon+\varepsilon'-\tilde{\varepsilon}_5-\tilde{\varepsilon}_6+i\sigma_5\delta}, \tag{13}$$

These expressions, like all the ones that follow, are written in the basis $\{\tilde{\phi}_1,\tilde{\varepsilon}_1\}$.

In what follows it will be shown that when several additional model constraints are imposed, the substitution of Eqs. (12) and (13) into (8) and (9) and later, taking into account (7), into (3) leads to the second random-phase approximation (SRPA) for $R(\omega)$ and some generalizations of it[2] (more precisely, we obtain the "uncorrelated" version of this model, which, as a rule, is what is used for calculations). The SRPA includes "pure" $2p2h$ configurations, although far from completely. The main advantages of this model are the systematic "microscopic" logic with which it is constructed and the correct inclusion of effects of second order in the interaction.

On the other hand, for nuclei the restriction to these effects is not well justified theoretically, because the perturbation series in the internucleon interaction $w$ can at best be viewed as asymptotic. From this point of view it is more correct to deal not with the individual terms of the perturbation series, but with partial sums of them containing an infinite number of terms, which would be accessible to actual calculation and at the same time would include the leading (in the magnitude of their contribution) sequences of terms of the initial series.

Unfortunately, there is no simple algorithm similar to that of perturbation theory which would permit solution of the problem of finding the complete set of all such partial sums and their correct use as the basic elements of the theory. However, the situation is simplified considerably if the model constructed in this manner contains a small parameter. In particular, in the case at hand of magic nuclei, we can find a small parameter if we take the solution of Eq. (3) for

the response function in the RPA as the partial sum of the terms of perturbation theory. This implies the introduction of phonons into the problem, with their energies $\omega_m$ coinciding with the poles of the response function $R(\omega)$ calculated in the RPA. The quasiparticle–phonon interaction amplitudes $g^m_{12}$ are determined by the residues of $R(\omega)$ at these poles.[15] In magic nuclei the amplitude $g$ itself is a small parameter.[43] More precisely, we should speak of the dimensionless quantity $\bar{g}=\langle j\|g\|j'\rangle/(\omega_m\sqrt{2j+1})$, where $j$ is the angular momentum of the quasiparticle with which the phonon interacts. Henceforth, when we say the amplitude $g$ is small it will be understood that $\bar{g}$ is small.

Here we shall not discuss the introduction of the phonon basis into the model,[40,41] or the formulation of this approach in the Green function method.[38,15,14] Let us give the final expressions for the functions $\Sigma^e$ and $\mathscr{U}^e$ in the simplest, i.e., the $g^2$ approximation:

$$\Sigma^e_{12}(\varepsilon)=\sum_{3,m}\frac{g^{m(\sigma_3)}_{13}*g^{m(\sigma_3)}_{23}}{\varepsilon-\tilde{\varepsilon}_3-\sigma_3(\omega_m-i\delta)}, \tag{14}$$

$$\mathscr{U}^e_{12,34}(\omega,\varepsilon,\varepsilon')=\sum_{\sigma,m}\frac{\sigma g^{m(\sigma)}_{31}*g^{m(\sigma)}_{42}}{\varepsilon-\varepsilon'+\sigma(\omega_m-i\delta)}, \tag{15}$$

where

$$g^{m(\sigma)}_{12}=\delta_{\sigma,+1}g^m_{12}+\delta_{\sigma,-1}g^{m*}_{21}. \tag{16}$$

The functions $\Sigma^e$ and $\mathscr{U}^e$ determined by (14) and (15), and also by (12) and (13), satisfy the identity

$$\Sigma^e_{12}(\varepsilon+\omega)-\Sigma^e_{12}(\varepsilon)=\int_{-\infty}^{\infty}\frac{d\varepsilon'}{2\pi i}\sum_{34}\mathscr{U}^e_{21,43}(\omega,\varepsilon,\varepsilon')\times[\tilde{G}_{34}(\varepsilon'+\omega)-\tilde{G}_{34}(\varepsilon')], \tag{17}$$

obtained from the dynamical consistency condition (10) by replacing the Green function $G$ on its right-hand side by $\tilde{G}$. The identity (17) plays an important role in the further model constructions.

As noted above, substitution of (14), (15) or (12), (13) into (8) and (9) and later into (7) and (3) takes us outside the RPA for the response function $R(\omega)$. More specifically, there are two variants of including $2p2h$ configurations in this quantity. Of course, this approach is limited by the approximations we have used for $\Sigma^e$ and $\mathscr{U}^e$. However, it can be anticipated that in magic nuclei, for which the amplitude $g$ is a small parameter, the $g^2$ approximation (14), (15) is good enough. It implies replacing "pure" $2p2h$ configurations by $1p1h\otimes$phonon configurations, which are coupled together because the phonon itself is a correlated superposition of $1p1h$ configurations. In the rest of our analysis we shall limit ourselves to this approximation, although most of the expressions remain valid for a wide class of functions $\Sigma^e$ and $\mathscr{U}^e$ if there are no special stipulations. In addition, we shall no longer assume that the mass operator $\tilde{\Sigma}$ is related to the amplitude $\tilde{\mathscr{U}}$ by any consistency conditions, because such conditions, although dictated by the requirements of a consistent microscopic theory, are in their known forms not adequate for the problem of including complex configurations and, moreover, they are not important for the methodological part of this exposition. The choice of $\tilde{\Sigma}$ (which in the simplest case corresponds to the phenomenological mean-field potential) and other quantities will be made specific when studying the applications of our approach.

### C. Renormalization of the equations for the response function

After choosing the approximations of the functions $\Sigma^e$ and $\mathscr{U}^e$, we are faced with the problem of finding the response function $R(\omega)$ using (2) and (3) with $G$ and $\mathscr{U}$ given by (7) and (9). The bulk of this review is devoted to the detailed analysis of one method of solving this problem. A fundamental difficulty in solving Eq. (3) for the function $R(\omega,\varepsilon)$ is that it is an integral over the energy variable $\varepsilon$, and both the kernel of this equation and its solution are singular functions of $\varepsilon$. It is useful to move this difficulty elsewhere, by introducing a new unknown function $R^e(\omega,\varepsilon)$ corresponding to the solution of an integral equation analogous to (3), which we shall write symbolically as

$$R^e=-GG+GG\mathscr{U}^eR^e. \tag{18}$$

The function $R^e(\omega,\varepsilon)$ thus defined allows us, using (9), to rewrite Eq. (3) for $R(\omega,\varepsilon)$ as

$$R=R^e-R^e\tilde{\mathscr{U}}R. \tag{19}$$

The reason for transforming to this equation is that, since the amplitude $\tilde{\mathscr{U}}$ is by definition independent of the energy variables, a known renormalization procedure[35] (more precisely, a variant[15] of it adapted to this type of equation) can be applied to (19). The result of this procedure is that the response function $R(\omega)$ is replaced by the renormalized response function $\tilde{R}(\omega)$ related to the original function as

$$R_{12,34}(\omega)=\sum_{5678}(\tilde{e}^+_q)_{12,56}\tilde{R}_{56,78}(\omega)(\tilde{e}_q)_{78,34}+\sum_{56}B_{12,56}(\tilde{e}_q)_{56,34} \tag{20}$$

and solving the equation

$$\tilde{R}_{12,34}(\omega)=A_{12,34}(\omega)-\sum_{5678}A_{12,56}(\omega)\tilde{\mathscr{F}}_{56,78}\tilde{R}_{78,34}(\omega). \tag{21}$$

In these expressions the effective charge operator $\tilde{e}_q$, the effective $p-h$ interaction amplitude $\tilde{\mathscr{F}}$, the generalized $p-h$ propagator $A(\omega)$, and the auxiliary quantity $B$ are given by

$$A_{12,34}(\omega)+B_{12,34}=\int_{-\infty}^{\infty}\frac{d\varepsilon}{2\pi i}R^e_{12,34}(\omega,\varepsilon), \tag{22}$$

$$\tilde{\mathscr{F}}_{12,34}=\sum_{56}(\tilde{e}_q)_{12,56}\tilde{\mathscr{U}}_{56,34}, \tag{23}$$

$$(\tilde{e}_q)_{12,34}=\delta_{13}\delta_{24}-\sum_{56}\tilde{\mathscr{F}}_{12,56}B_{56,34}=(\tilde{e}^+_q)^*_{34,12}. \tag{24}$$

We stress the fact that the transformation $R\to\tilde{R}$ specified by (20)–(24) is formally exact. An additional hypothesis is that

the quantity $B$ on the left-hand side of (22) is independent of the energy variable $\omega$. Obviously, if $B$ is independent of the variable $\omega$, the quantities $\tilde{e}_q$ and $\tilde{\mathcal{F}}$ possess the same property.[4)] In addition, it is assumed that $B$ is relatively small, so that the operator $\tilde{e}_q$ is close to unity.

The meaning of the auxiliary quantity $B$ is defined by (22): it includes all the contributions of partial sums of terms of the rearranged perturbation series which enter into the integral of the function $R^e(\omega,\varepsilon)$ on the right-hand side of (22), but are not included in the generalized $p-h$ propagator $A(\omega)$. We have not yet rigorously defined this propagator, but it is obvious that it must be constructed such that the hypothesis that $B$ is relatively small and independent of $\omega$ is justified. In other words, the function $A(\omega)$ must approximate the integral on the right-hand side of (22) sufficiently well. As far as $\tilde{e}_q$ and $\tilde{\mathcal{F}}$ are concerned, in the applications of this approach studied below they are parametrized as in the theory of finite Fermi systems.[35]

Since $B$ is independent of the energy variable, it follows from (20) and (1) that $S(E)=\lim_{\Delta\to+0}S(E,\Delta)$, where

$$S(E,\Delta)=\frac{1}{\pi}\,\mathrm{Im}\sum_{1234}(\tilde{e}_qV^0)^*_{21}\tilde{R}_{12,34}(E+i\Delta)(\tilde{e}_qV^0)_{43}, \tag{25}$$

$$(\tilde{e}_qV^0)_{12}=\sum_{34}(\tilde{e}_q)_{21,43}V^0_{34}, \tag{26}$$

i.e., the strength function is completely determined by the renormalized response function $\tilde{R}(\omega)$.

As a result of these transformations, the difficulty of solving the integral equation in the energy variable is transferred from Eq. (3) for the function $R(\omega,\varepsilon)$ to Eq. (18) for the function $R^e(\omega,\varepsilon)$, which according to (22) determines, up to $B$, the generalized $p-h$ propagator $A(\omega)$ up to $B$ and then, via Eq. (21), the renormalized response function $\tilde{R}(\omega)$. However, in contrast to the original situation, the problem is simpler because now we do not need to solve (18) exactly, but can try to replace it by an approximate equation for the function $A(\omega)$, which would be an algebraic equation in the energy variable. The departure from the exact solution is compensated for by the auxiliary quantity $B$, i.e., ultimately by the parameters which determine the effective quantities $\tilde{e}_q$ and $\tilde{\mathcal{F}}$.

## 3. THE PRINCIPLE OF TIME-ORDERED GRAPH DECOUPLING

In this section we shall study the technical aspects of the method we use to construct the generalized $p-h$ propagator $A(\omega)$. The rigorous formulation and physical justification of the method will be discussed in the next section. Since many of the expressions given below will be written in the time ($t$) representation, for brevity we shall, as in Eq. (4) above, use boldface numbers to denote the set of one-particle quantum numbers and the time variable: $1=\{1,t_1\}$ and so on. In particular, the Green function $\tilde{G}$ given by (11) becomes

$$\tilde{G}(1,2)=-i\sigma_1\delta_{12}\theta(\sigma_1t_{12})e^{-i\tilde{\varepsilon}_1t_{12}} \tag{27}$$

in this representation, where $t_{12}=t_1-t_2$ and $\theta$ is the Heaviside (step) function.[42]

Let us consider the integral operator in the $t$ representation whose matrix elements in the basis $\{\tilde{\phi}_1,\tilde{\varepsilon}_1\}$ are given by

$$\tilde{D}(12,34)=\delta_{\sigma_1,-\sigma_2}\theta(\sigma_1t_{41})\theta(\sigma_1t_{32})\tilde{G}(3,1)\tilde{G}(2,4). \tag{28}$$

Multiplying the right-hand side of (28) by the sum $\theta(\sigma_1t_{12})+\theta(\sigma_1t_{21})\equiv1$ and using (27), we find

$$\begin{aligned}\tilde{D}(12,34)=\delta_{\sigma_1,-\sigma_2}\delta_{13}\delta_{24}e^{-i(\tilde{\varepsilon}_1t_{31}+\tilde{\varepsilon}_2t_{24})}\\ \times[\theta(\sigma_1t_{12})\theta(\sigma_1t_{41})\theta(\sigma_1t_{31})\\ +\theta(\sigma_1t_{21})\theta(\sigma_1t_{32})\theta(\sigma_1t_{42})].\end{aligned} \tag{29}$$

In deriving this equation we have used the easily verified identity ($\sigma=\pm1$)

$$\theta(\sigma t_{13})\theta(\sigma t_{12})\theta(\sigma t_{23})=\theta(\sigma t_{12})\theta(\sigma t_{23}). \tag{30}$$

We introduce, using the notation of Ref. 15, the time-difference variables

$$\tilde{D}(12,34)\equiv\tilde{D}_{12,34}(\tau_1,\tau_2,\tau_3),$$

$$\tau_1=t_{31},\quad \tau_2=t_{21},\quad \tau_3=t_{34}$$

and transform to the energy representation using the expression

$$\begin{aligned}\tilde{D}_{12,34}(\omega,\varepsilon,\varepsilon')=\int_{-\infty}^{\infty}d\tau_1d\tau_2d\tau_3e^{i(\omega\tau_1+\varepsilon\tau_2+\varepsilon'\tau_3)}\\ \times\tilde{D}_{12,34}(\tau_1,\tau_2,\tau_3).\end{aligned} \tag{31}$$

Substituting (29) into (31) and using the well-known expression

$$\int_{-\infty}^{\infty}d\tau e^{i\omega\tau}\theta(\sigma\tau)=\frac{i\sigma}{\omega+i\sigma\delta},\quad \sigma=\pm1,\quad \delta\to+0, \tag{32}$$

we find

$$\begin{aligned}\tilde{D}_{12,34}(\omega,\varepsilon,\varepsilon')=\delta_{\sigma_1,-\sigma_2}\delta_{13}\delta_{24}\\ \times\frac{i\sigma_1}{(\varepsilon'+\omega-\tilde{\varepsilon}_1+i\sigma_1\delta)(\varepsilon'-\tilde{\varepsilon}_2+i\sigma_2\delta)}\\ \times\left(\frac{1}{\varepsilon+\omega-\tilde{\varepsilon}_1+i\sigma_1\delta}-\frac{1}{\varepsilon-\tilde{\varepsilon}_2+i\sigma_2\delta}\right).\end{aligned}$$

From this, using the definitions (11) we obtain the final result:

$$\begin{aligned}\tilde{D}_{12,34}(\omega,\varepsilon,\varepsilon')=-i\delta_{\sigma_1,-\sigma_2}\delta_{13}\delta_{24}\sigma_1(\omega-\tilde{\varepsilon}_{12}+i\sigma_1\delta)\\ \times\tilde{G}_1(\varepsilon+\omega)\tilde{G}_2(\varepsilon)\tilde{G}_3(\varepsilon'+\omega)\tilde{G}_4(\varepsilon').\end{aligned} \tag{33}$$

We see from this expression that the dependence of the function $\tilde{D}(\omega,\varepsilon,\varepsilon')$ on the variables $\varepsilon$ and $\varepsilon'$ is separable. This is essential for the further model transformations. We note

that the simple product of two Green functions $\tilde{R}^0(12,34)=-\tilde{G}(3,1)\tilde{G}(2,4)$, which in the energy representation is given by

$$\tilde{R}^{0}_{12,34}(\omega,\varepsilon,\varepsilon')=-\delta_{13}\delta_{24}2\pi\delta(\varepsilon-\varepsilon')\tilde{G}_1(\varepsilon+\omega)\tilde{G}_2(\varepsilon)$$

does not possess this property.

In order to understand the effect of this separability, let us consider a function $F(12,34)$, which in the $t$ representation is given by the contraction

$$F(12,34)=\frac{1}{i}\sum_{5678}^{t} V^L(12,56)\tilde{D}(56,78)V^R(78,34), \tag{34}$$

where $V^L$ and $V^R$ are different functions whose dependence on the time arguments reduces to dependence on three time-difference variables:

$$V^L(12,34)=V^L_{12,34}(t_{31},t_{21},t_{34}),$$
$$V^R(12,34)=V^R_{12,34}(t_{31},t_{21},t_{34});$$

and $\Sigma'_{12\ldots}$ denotes summation over the one-particle indices of the basis wave functions $\tilde{\phi}_1$ and integration over the time variables:

$$\sum_{12\ldots}^{t}\equiv\sum_{12\ldots}\int_{-\infty}^{\infty}dt_1dt_2\ldots .$$

Writing (34) in the energy representation, defined analogously to (31), we obtain

$$F_{12,34}(\omega,\varepsilon,\varepsilon')=\frac{1}{i}\sum_{5678}\int_{-\infty}^{\infty}\frac{d\varepsilon_1 d\varepsilon_2}{(2\pi)^2}V^L_{12,56}(\omega,\varepsilon,\varepsilon_1)\times\tilde{D}_{56,78}(\omega,\varepsilon_1,\varepsilon_2)V^R_{78,34}(\omega,\varepsilon_2,\varepsilon'). \tag{35}$$

Substituting Eq. (33) into this, we see that, owing to the separability of the energy dependence of $\tilde{D}(\omega,\varepsilon_1,\varepsilon_2)$, the integrations over the variables $\varepsilon_1$ and $\varepsilon_2$ in (35) decouple. From the purely technical point of view this is due to the presence of the additional (compared to $\tilde{R}^0$) factor of two $\theta$ functions on the right-hand side of (28) expressing the function $\tilde{D}$ in the $t$ representation. The replacement of $\tilde{R}^0$ by $-\tilde{D}$ in the expressions determining the generalized $p-h$ propagator is the main element (principle) of the method of constructing it in our approach. The physical meaning of this principle is clear from the interpretation of the quantities entering into equations like (34) and (35), and in terms of Feynman diagrams. This effect also provides the name of the principle itself, and indeed of our entire approach, which we refer to as the method of time-ordered graph decoupling (the TOGD method).

## 4. THE PARTICLE–HOLE PROPAGATOR IN THE TOGD METHOD

For the rest of the analysis we shall need to distinguish between particle ($p$) and hole ($h$) indices of the matrix elements of integral operators like $F_{12,34}$ (in terms of the one-particle indices of the basis $\{\tilde{\phi}_1,\tilde{\varepsilon}_1\}$, for which the index introduced earlier is $\sigma_p=+1$ for particles and $\sigma_h=-1$ for holes). We shall refer to a pair of one-particle indices {1,2} as a pair of *unlike* indices if it is a $p-h$ or an $h-p$ pair (i.e., $1=p$, $2=h$ or $1=h$, $2=p$). If the pair {1,2} is a $p-p'$ or an $h-h'$ pair, we shall refer to it as a pair of *like* indices. Setting by definition $\sigma_{12}=\sigma_1\sigma_2$, we see that for a pair of unlike indices {1,2} we always have $\sigma_{12}=-1$, while for a pair of like indices we always have $\sigma_{12}=+1$.

Using this terminology, let us divide the matrix elements $F_{12,34}$ into 3 classes: (1) both pairs of indices {1,2} and {3,4} are unlike; (2) both pairs of indices {1,2} and {3,4} are like; (3) one of the pairs of indices {1,2} and {3,4} is unlike and the other is like. In the first case the matrix element $F_{12,34}$ will be termed the *unlike* component of $F$, in the second it will be the *like* component, and in the third it will be the *mixed* component.

These definitions can be formalized as follows. Let $F$ be given by its matrix elements $F_{12,34}$. We introduce the four quantities $F^{(--)}$, $F^{(-+)}$, $F^{(+-)}$, and $F^{(++)}$, taking

$$F^{(\sigma,\sigma')}_{12,34}=\delta_{\sigma,\sigma_{12}}\delta_{\sigma',\sigma_{34}}F_{12,34}, \tag{36}$$

where $\sigma=\pm1$, $\sigma'=\pm1$, $\sigma_{12}=\sigma_1\sigma_2$, and $\sigma_{34}=\sigma_3\sigma_4$. Obviously, $F^{(--)}$ has only unlike components, $F^{(++)}$ has only like ones, and $F^{(-+)}$ and $F^{(+-)}$ have only mixed ones. In addition, from (36) we find

$$F_{12,34}=F^{(--)}_{12,34}+F^{(-+)}_{12,34}+F^{(+-)}_{12,34}+F^{(++)}_{12,34}. \tag{37}$$

We shall introduce a special single term for the like and mixed components, referring to them as the *associated* components. The meaning of this term is clear from the decomposition (37): the like and mixed components are associated with the unlike components $F^{(--)}$, the entire set forming the original quantity $F$. The unlike components are singled out in this classification owing to the fact that $F$ has only unlike components in the RPA, which is the simplest approximation for the object of our model, the response function $R_{12,34}$.

### 4.1. The fundamental condition for the propagator of the TOGD method

Let us turn to the solution of the central problem of this approach: the use of the TOGD method for constructing the generalized $p-h$ propagator $A(\omega)$. This method, based on the principle of time-ordered graph decoupling, was proposed in Ref. 18 and realized in the model including $1p1h\otimes$phonon configurations (Refs. 17, 18, 27–34, and 36). Here we present it in a form more general than in Ref. 18, which allows the propagator $A(\omega)$ to be constructed in a larger class of models determined by the specific choice of the mass operator $\Sigma^e$ and the interaction amplitude $\mathcal{V}^e$.

We begin by transforming Eq. (18) for the function $R^e$, which according to (22) must determine the desired propagator $A(\omega)$. Acting on both sides of (18) with the operator $(G^{-1}\tilde{G})(\tilde{G}G^{-1})$ and then using (7), in the $t$ representation we obtain

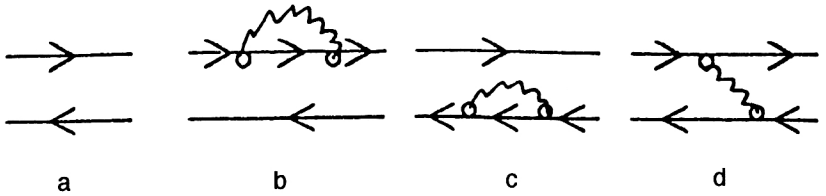


FIG. 1. Graphs corresponding to the function $A^{(1)}(\omega)$ in the model including $1p1h\otimes$phonon configurations. The wavy line and the circle denote the phonon Green function and the amplitude $g$, and the thin lines denote the Green function $\tilde{G}$. Graph a corresponds to the function $A^{[0]}(\omega)$, and graphs b, c, and d correspond to the function $A^{[1]}(\omega)$.

$$R^e(12,34)=\tilde{R}^0(12,34)+i\sum_{5678}^{t}\tilde{R}^0(12,56)\mathscr{V}^v(56,78)R^e(78,34), \tag{38}$$

where

$$\tilde{R}^0(12,34)=-\tilde{G}(3,1)\tilde{G}(2,4), \tag{39}$$

$$\mathscr{V}^v(12,34)=W^e(12,34)-i\Sigma^e(3,1)\Sigma^e(2,4), \tag{40}$$

$$W^e(12,34)=\mathscr{U}^e(12,34)+i\Sigma^e(3,1)\tilde{G}^{-1}(2,4)+i\tilde{G}^{-1}(3,1)\Sigma^e(2,4). \tag{41}$$

The term $-\Sigma^e\Sigma^e$ on the right-hand side of (40), which arises as a result of formal identity transformations, plays the role of a cancellation term which eliminates the multiple counting of graphs with self-energy insertions in the diagrammatic expansion of $R^e$.

To formulate the main condition which we shall impose on the function $A(\omega)$, we introduce the auxiliary parameter $\alpha$, making the following replacements in (40) and (41):

$$\Sigma^e\to\alpha\Sigma^e,\quad \mathscr{U}^e\to\alpha\mathscr{U}^e. \tag{42}$$

These replacements lead to the appearance of an $\alpha$ dependence of $R^e$, for which we obtain the following expansion in the energy representation:

$$\int_{-\infty}^{\infty}\frac{d\varepsilon}{2\pi i}R^e_{12,34}(\omega,\varepsilon)=\sum_{n=0}^{\infty}R^{e[n]}_{12,34}(\omega)\alpha^n. \tag{43}$$

The coefficients of this expansion $R^{e[n]}$ are easily found by solving (38) iteratively. Since we assume that the desired propagator $A(\omega)$ as a function of $R^e$ must be uniquely determined by $\Sigma^e$ and $\mathscr{U}^e$, we have an expansion analogous to (43) for it:

$$A_{12,34}(\omega)=\sum_{n=0}^{\infty}A^{[n]}_{12,34}(\omega)\alpha^n. \tag{44}$$

Our condition is that the first two coefficients of the expansions (43) and (44) coincide:

$$A^{[0]}_{12,34}(\omega)=R^{e[0]}_{12,34}(\omega),\quad A^{[1]}_{12,34}(\omega)=R^{e[1]}_{12,34}(\omega). \tag{45}$$

This condition is quite natural in the model including $1p1h\otimes$phonon configurations, where the functions $\Sigma^e$ and $\mathscr{U}^e\sim g^2$ [Eqs. (14) and (15)], and so $R^{e[n]}$ and $A^{[n]}\sim g^{2n}$, i.e., the values of the other ($n\geq 2$) coefficients of the expansions (43) and (44) must be small. The question arises of whether or not we can restrict ourselves to the coefficients $A^{[0]}$ and $A^{[1]}$ in this case, taking the desired propagator to be (here and below in the final expressions we set $\alpha=1$)

$$A^{(1)}_{12,34}(\omega)=A^{[0]}_{12,34}(\omega)+A^{[1]}_{12,34}(\omega).$$

In Fig. 1 we show the Feynman graphs corresponding to the function $A^{(1)}_{12,34}(\omega)$. Unfortunately, this simple solution, which is the propagator of the model of Ref. 14, leads to the following problem: the unlike components of $A^{[1]}_{12,34}(\omega)$ and $A^{(1)}_{12,34}(\omega)$ contain poles of second order in the variable $\omega$ at the points of the simple poles of the function $A^{[0]}_{12,34}(\omega)$. The problem is that the second-order poles do not have the same physical meaning as the simple poles of the exact response function, which is partially expressed by (1). This can result in distortion of the energy dependence of the strength function near these poles.

The way out of this difficulty is to approximately include the sum of the remaining terms of the expansion in (43). The resulting elimination of second-order poles in $\omega$ can be illustrated by the simple example of exactly summing the infinite series of terms of the geometrical progression $f(\omega)=a(\omega)\Sigma_{n=0}^{\infty}(\alpha a(\omega))^n$, where $a$ is a pole function of $\omega$: $a(\omega)=c/(\omega-\omega_0)$. This sum has a simple pole in $\omega$ which is shifted relative to the pole of the function $a(\omega)$ by an amount $c\alpha$: $f(\omega)=c/(\omega-\omega_0-c\alpha)$. On the other hand, restricting ourselves to the first two terms of this sum, we obtain the function

$$f^{(1)}(\omega)=\frac{c}{\omega-\omega_0}+\frac{c^2\alpha}{(\omega-\omega_0)^2},$$

which contains a second-order pole at the pole of the function $a(\omega)$ and in this sense is analogous to the function $A^{(1)}(\omega)$.

### 4.2. Farmulation of the method

Briefly stated, the use of the TOGD method to approximately sum the series (43) amounts to the following. Using symbolic notation, we write the solution of (38) in the form

$$R^e=\tilde{R}^0+i\tilde{R}^0\Gamma^e\tilde{R}^0, \tag{46}$$

where the amplitude $\Gamma^e$ is the solution of the equation

$$\Gamma^e=\mathscr{V}^v+i\mathscr{V}^v\tilde{R}^0\Gamma^e. \tag{47}$$

We introduce the new amplitude $\tilde{\Gamma}^e$ defined by the equation

$$\tilde{\Gamma}^e=\tilde{\mathscr{V}}^v+i\tilde{\mathscr{V}}^v(-\tilde{D})\tilde{\Gamma}^e, \tag{48}$$

which is obtained from (47) by the replacement

$$\tilde{R}^0\to-\tilde{D},\quad \mathscr{V}^v\to\tilde{\mathscr{V}}^v. \tag{49}$$

Here the function $\tilde{D}$ is given by (28), and the amplitude $\tilde{\mathscr{V}}^v$ is given by

$$\tilde{\mathscr{V}}^v(12,34)=W^e(12,34)+W^{\text{comp}}(12,34), \tag{50}$$

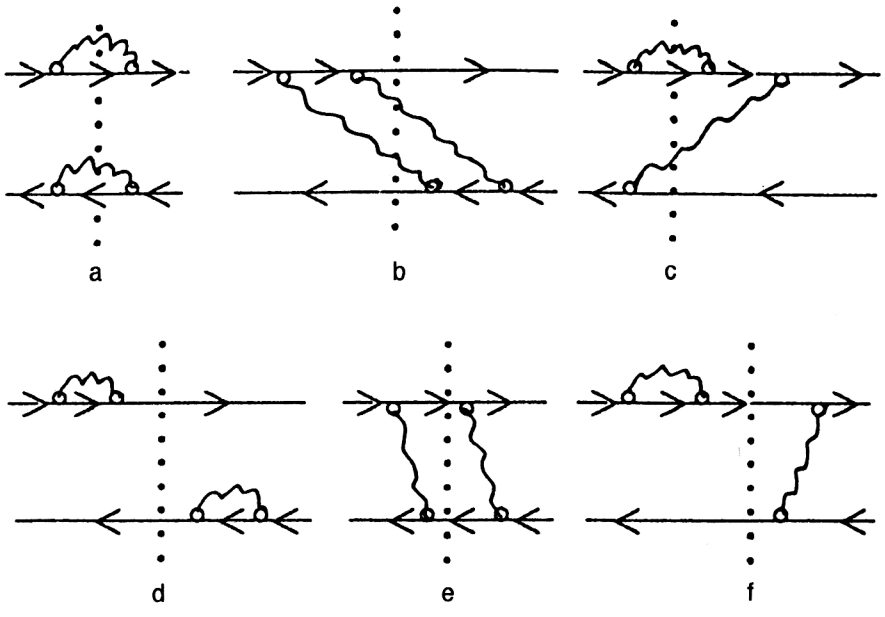


FIG. 2. Typical graphs of fourth order in the quasiparticle–phonon interaction amplitude $g$ entering into the diagrammatic expansion of the function $R^e$ in the $t$ representation. The notation is the same as in Fig. 1, but here the direction of the arrow on a fermion line denotes the particle ($\rightarrow -$.) or hole ($-\leftarrow$.) Green function $\tilde{G}$. The dotted line denotes the time cut at fixed time $t$. Only graphs d, e, and f are explicitly included in the TOGD method.

which differs from (40) by the replacement of $-i\Sigma^e\Sigma^e$ by $W^{\text{comp}}$. The amplitude $W^{\text{comp}}$ in (50) plays the same cancellation role as the term $-i\Sigma^e\Sigma^e$ in (40), and will be defined below. Now in (46) we replace the amplitude $\Gamma^e$ by $\tilde{\Gamma}^e$:

$$\tilde{R}^e=\tilde{R}^0+i\tilde{R}^0\tilde{\Gamma}^e\tilde{R}^0. \tag{51}$$

After transforming to the energy representation, this function defines the desired propagator:

$$A_{12,34}(\omega)=\int_{-\infty}^{\infty}\frac{d\varepsilon}{2\pi i}\tilde{R}^e_{12,34}(\omega,\varepsilon). \tag{52}$$

Let us see if these model transformations are correct. Taking into account the fact that in the replacement (42) the amplitude $W^{\text{comp}}\sim\alpha^2$ [see Eq. (54) below], it is easily verified that the propagator $A(\omega)$ constructed in this manner satisfies the fundamental condition (45). In addition, representing the solution of the integral equation (48) as a Neumann series

$$\tilde{\Gamma}^e=\tilde{\mathscr{W}}^v\sum_{n=0}^{\infty}(-i\tilde{D}\tilde{\mathscr{W}}^v)^n$$

and then making the replacement (42), we see that the function $\tilde{R}^e$ and, consequently, the propagator $A$, contain an infinite sum of terms of higher order in the auxiliary parameter $\alpha$. An additional condition, whose fulfillment must be verified, is that this sum must correspond to a series of Feynman graphs whose terms form a subset of the set of terms of the graphs corresponding to the initial quantity $R^e$. This is a physical condition, because each Feynman graph describes a certain physical process, even though it is not necessarily physically observable. This implies that we should not include in $\tilde{R}^e$ processes which are not contained in $R^e$, while included processes should be included only once.

In this sense the replacement of $\tilde{R}^0$ by $-\tilde{D}$ is justified by the fact that, according to (28) and (39), the quantity $-\tilde{D}$ has only unlike components and differs from $\tilde{R}^{0(--)}$ by only an additional factor consisting of $\theta$ functions, which are projection operators in the space of time variables, i.e., the graphs corresponding to different combinations of arguments of the function $-\tilde{D}(12,34)$ belong to the set of graphs corresponding to the function $\tilde{R}^0(12,34)$. However, from the physical point of view it is just as important that the replacement of $\tilde{R}^0$ by $-\tilde{D}$ eliminates from the diagrammatic expansion of $R^e$ the terms corresponding to processes in which configurations more complex than $2p2h$ are excited,[5] while leaving most of the $2p2h$ configurations. In the model including $1p1h\otimes$phonon configurations, the discarded graphs also include those in which a time cut through two or more phonon lines is possible in the $t$ representation. As an example, in Figs. 2a and 2b we give three graphs of this type of fourth order in $g$, and in Figs. 2d, 2e, and 2f we give three similar graphs which remain in the diagrammatic expansion of $\tilde{R}^e$. The sum of the contributions of higher order in the amplitude $g$, which is contained in the function $\tilde{R}^e$ (i.e., contributions $\sim g^{2n}$, $n\geqslant 3$) corresponds to the sum of chains of graphs similar to those shown in Figs. 2d, 2e, and 2f. The contributions of the graphs shown in Figs. 2a, 2b, and 2c are excluded by the $\theta$ functions entering into the definition of $\tilde{D}$, which makes the formal transformation (49) physically correspond to a graph selection principle.

It should be noted that the statement that in the TOGD method all contributions of configurations more complex than $2p2h$ are excluded, while all $2p2h$ contributions are included, is not rigorous even in the hypothetical case where the quantities $\Sigma^e$ and $\mathscr{W}^e$ are determined exactly. Within the approximations (12), (13) or (14), (15) for $\Sigma^e$ and $\mathscr{W}^e$ this statement is completely valid only when ground-state correlation effects are ignored; the role played by these effects will be discussed in detail below. These effects correspond to so-called backward-running graphs, and their inclusion in the TOGD method, on the one hand, takes us beyond the $2p2h$ approximation (in Fig. 3 we give some graphs of this type with self-energy insertions). On the other hand, it means that not all the $2p2h$ contributions related to them (of order

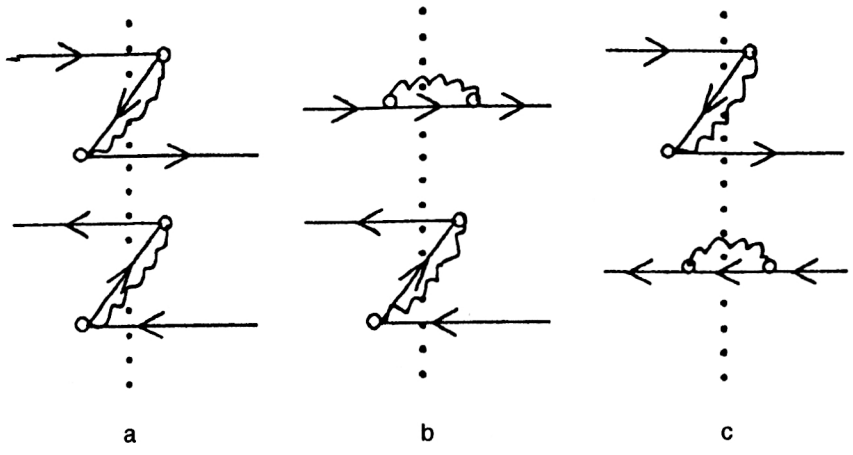


FIG. 3. Graphs of order $g^4$ with self-energy insertions in the $t$ representation which are included in the TOGD method and arise from ground-state correlation effects. The notation is the same as in Fig. 2.

$g^4$ and above) are included. However, since $g$ is a small parameter, these neglected contributions are small.

### 4.3. Cancellation of multiple counting of graphs

Let us now consider the problem of finding the amplitude $W^{\text{comp}}$ in (50). As already mentioned, its role is to remove (cancel) the multiple counting of graphs with self-energy insertions. In the TOGD method this problem arises only for the coefficients of the expansion (44), $A^{[n]}(\omega)$, with $n \geqslant 2$ and only with the inclusion of ground-state correlations, i.e., backward-running graphs like those shown in Fig. 3 (for brevity, we shall refer to graphs containing at least one Z-like fermion line as Z-graphs; however, they represent only one type of backward-running graph). In the absence of Z-graphs, multiple counting is eliminated by the $\theta$ functions entering into the definition of $\tilde{D}$, and so in this case $W^{\text{comp}} \equiv 0$. It follows from this that in general this amplitude should differ from $-i\Sigma^e\Sigma^e$, which it replaces in the TOGD method. In this method $W^{\text{comp}}$ is determined from the condition of cancellation of the double counting of self-energy contributions in the coefficient $A^{[2]}(\omega)$ of the expansion (44). If we set $W^{\text{comp}} \equiv 0$, then according to Eqs. (41), (48), and (50)–(52) double counting arises only in the part of the amplitude $\tilde{\Gamma}^e$ consisting of the sum of the two terms obtained after the first iteration of (48). Denoting this part $\tilde{\Gamma}^{e(dc)}$, in the $t$ representation we have

$$\tilde{\Gamma}^{e(dc)} = i(i\Sigma^e\tilde{G}^{-1})(-\tilde{D})(i\tilde{G}^{-1}\Sigma^e) + i(i\tilde{G}^{-1}\Sigma^e)(-\tilde{D}) \times (i\Sigma^e\tilde{G}^{-1}).$$

In detailed notation this expression is

$$\begin{aligned}\tilde{\Gamma}^{e(dc)}(12,34) &= i\sum_{1'2'3'4'}^{t}\sum_{5'6'7'8'}^{t}\delta_{\sigma_1,-\sigma_2}\delta_{\sigma_3,-\sigma_4}\delta_{\sigma_{1'},-\sigma_{4'}} \\ &\times\tilde{G}^{-1}(1',1)\tilde{G}(5',1')\tilde{G}^{-1}(2,2') \\ &\times\times\tilde{G}(2',6')\Sigma^e(7',5')\Sigma^e(6',8') \\ &\times\tilde{G}(3',7')\tilde{G}^{-1}(3,3')\tilde{G}(8',4')\tilde{G}^{-1}(4',4) \\ &\times[\theta(\sigma_1 t_{4'1'})\theta(\sigma_1 t_{5'8'}) + \theta(\sigma_{1'} t_{3'2'})\theta(\sigma_1 t_{6'7'})].\end{aligned}$$

Treating the $\theta$ functions in this equation as projection operators acting in an 8-dimensional linear space whose coordinates are the variables $t_{1'}, t_{2'}, \ldots, t_{8'}$, we find that there is double counting of only the region of this space obtained by projection with the operator

$$\Theta(1'2',3'4') = \theta(\sigma_{1'} t_{4'1'})\theta(\sigma_{1'} t_{5'8'}) \times \theta(\sigma_{1'} t_{3'2'})\theta(\sigma_{1'} t_{6'7'}), \tag{53}$$

which is the product of all the projection operators enclosed in the square brackets. From this we find that, according to (48) and (50), this double counting in the function $A^{[2]}(\omega)$ can be eliminated using the amplitude

$$\begin{aligned}W^{\text{comp}}(12,34) = -i\delta_{\sigma_1,-\sigma_2}\delta_{\sigma_3,-\sigma_4}\delta_{\sigma_1,\sigma_3}\sum_{1'2'3'4'}^{t}\sum_{5'6'7'8'}^{t} \\ \times\tilde{G}^{-1}(1',1)\tilde{G}(5',1')\tilde{G}^{-1}(2,2') \\ \times\tilde{G}(2',6')\Sigma^e(7',5')\Sigma^e(6',8') \\ \times\tilde{G}(3',7')\tilde{G}^{-1}(3,3')\tilde{G}(8',4') \\ \times\tilde{G}^{-1}(4',4)\Theta(1'2',3'4').\end{aligned} \tag{54}$$

This expression was used in Ref. 18 as the definition of $W^{\text{comp}}$. We note that if the Z-part of the mass operator $\Sigma^e$ is given in the $t$ representation by

$$\Sigma^{e(Z)}(1,2) = \delta_{\sigma_1,\sigma_2}\theta(\sigma_1 t_{21})\Sigma^e(1,2), \tag{55}$$

then from (54), (30), and the obvious identity $\theta(\tau)\theta(-\tau) \equiv 0$ it follows that $W^{\text{comp}} \equiv 0$ if none of the mass operators $\Sigma^e$ entering into (54) contains Z-graphs. Since it is the operators $\Sigma^{e(Z)}$ which generate Z-like fermion lines, this property of the expression for $W^{\text{comp}}$ forms the basis of the assertion that there is no multiple counting of graphs in the TOGD method when Z-graphs are excluded and $W^{\text{comp}} \equiv 0$.

### 4.4. The propagator of the TOGD method in the energy representation

Equations (28), (39), (41), (48), and (50)–(54) completely determine the generalized $p-h$ propagator $A(\omega)$ in the TOGD method. However, since all of them, except (52),

are written in the $t$ representation, it is necessary to transform to the energy representation. After some algebra, which for brevity we omit, we obtain

$$A_{12,34}(\omega)=\sum_{5678}[\delta_{15}\delta_{26}+Q^{(+-)}_{12,56}(\omega)]A^{(--)}_{56,78}(\omega)[\delta_{73}\delta_{84}+Q^{(-+)}_{78,34}(\omega)]+P^{(++)}_{12,34}(\omega), \tag{56}$$

where

$$Q^{(+-)}_{12,34}(\omega)=-\delta_{\sigma_1,\sigma_2}\delta_{\sigma_3,-\delta_4}A^{[1]}_{12,34}(\omega)\sigma_3(\omega-\tilde{\varepsilon}_{34}), \tag{57}$$

$$Q^{(-+)}_{12,34}(\omega)=-\delta_{\sigma_1,-\sigma_2}\delta_{\sigma_3,\sigma_4}\sigma_1(\omega-\tilde{\varepsilon}_{12})A^{[1]}_{12,34}(\omega), \tag{58}$$

$$P^{(++)}_{12,34}(\omega)=\delta_{\sigma_1,\sigma_2}\delta_{\sigma_3,\sigma_4}A^{[1]}_{12,34}(\omega), \tag{59}$$

$$\begin{aligned}A^{[1]}_{12,34}(\omega)=&-\int_{-\infty}^{\infty}\frac{d\varepsilon d\varepsilon'}{(2\pi i)^2}\tilde{G}_1(\varepsilon+\omega)\\&\times\tilde{G}_2(\varepsilon)\mathscr{V}^{e}_{12,34}(\omega,\varepsilon,\varepsilon')\tilde{G}_3(\varepsilon'+\omega)\\&\times\tilde{G}_4(\varepsilon')-\int_{-\infty}^{\infty}\frac{d\varepsilon}{2\pi i}[\delta_{31}\tilde{G}_1(\varepsilon+\omega)\\&\times\tilde{G}_2(\varepsilon)\Sigma^{e}_{24}(\varepsilon)\tilde{G}_4(\varepsilon)+\delta_{24}\tilde{G}_3(\varepsilon+\omega)\\&\times\Sigma^{e}_{31}(\varepsilon+\omega)\tilde{G}_1(\varepsilon+\omega)\tilde{G}_2(\varepsilon)],\end{aligned} \tag{60}$$

$\tilde{\varepsilon}_{12}=\tilde{\varepsilon}_1-\tilde{\varepsilon}_2$, and the Green function $\tilde{G}_1(\varepsilon)$ is given by (11). The only equation which must be solved to find the propagator $A(\omega)$ is the equation for its unlike components:

$$A^{(--)}_{12,34}(\omega)=\tilde{A}_{12,34}(\omega)-\sum_{5678}\tilde{A}_{12,56}(\omega)\Phi_{56,78}(\omega)A^{(--)}_{78,34}(\omega), \tag{61}$$

in which

$$\tilde{A}_{12,34}(\omega)=-\delta_{13}\delta_{24}\sigma_1\delta_{\sigma_1,-\sigma_2}/(\omega-\tilde{\varepsilon}_{12}), \tag{62}$$

$$\Phi_{12,34}(\omega)=\tilde{\Phi}_{12,34}(\omega)+\Phi^{\mathrm{comp}}_{12,34}(\omega), \tag{63}$$

$$\begin{aligned}\tilde{\Phi}_{12,34}(\omega)=&-\delta_{\sigma_1,-\sigma_2}\delta_{\sigma_3,-\sigma_4}\sigma_1(\omega-\tilde{\varepsilon}_{12})\\&\times A^{[1]}_{12,34}(\omega)\sigma_3(\omega-\tilde{\varepsilon}_{34}).\end{aligned} \tag{64}$$

The function $A^{[1]}(\omega)$ appearing in these expressions is, as it is denoted, a coefficient in the expansion (44). In addition, the function $\tilde{A}(\omega)$ in (61) coincides with the coefficient $A^{[0]}(\omega)$ of this expansion and is therefore the $p-h$ propagator in the RPA obtained from (44) for $\alpha=0$.

### 4.5. The expression for $\Phi^{\mathrm{comp}}$

The amplitude $\Phi^{\mathrm{comp}}(\omega)$ in (63) is responsible for canceling the multiple counting of graphs with self-energy insertions and is uniquely determined by the expression for $W^{\mathrm{comp}}$. However, the direct use of Eq. (54) for $W^{\mathrm{comp}}$ generates false poles in $\Phi^{\mathrm{comp}}(\omega)$, i.e., poles which are not present in the function $R^{e[2]}(\omega)$ and which can be referred to as $4p4h$ poles [Eq. (24) of Ref. 18, in which the model including $1p1h\otimes$phonon configurations was used, with the notation $\Phi^{(2)}\equiv\tilde{\Phi}$, $\Phi^{(4)}\equiv\Phi^{\mathrm{comp}}$]. The appearance of these poles is related to the fact that when one of the mass operators in the amplitude $\tilde{\Gamma}^{e(dc)}$ defined above does not contain Z-like parts, while the other does, $\Sigma^e=\Sigma^{e(\mathrm{Z})}$ (as, for example, in the graphs of Figs. 3b and 3c), the double counting is no more important than the other effects of second order in the auxiliary parameter $\alpha$ in the expansion (43), which are neglected in the TOGD method. Using the fact that in the model including $1p1h\otimes$phonon contributions the contributions of all these effects are of order $g^4$, it is permissable to simply dispense with the cancellation of double counting in this case, thereby discarding the pole part of $\Phi^{\mathrm{comp}}(\omega)$.

As an additional argument, we note that, according to Eqs. (21), (56), and (61)–(63), the pole part of $\Phi^{\mathrm{comp}}(\omega)$ (in contrast to the nonpole parts of this function) does not contribute to the first two terms of the expansion of the response function $\tilde{R}(\omega)$ in powers of $1/\omega$, so that its elimination in any case does not affect the moments of the strength function, $m_0$ and $m_1$, associated with this expansion (see Ref. 11) in the TOGD method. This approximation implies cancellation of the double counting of the contributions from only those graphs corresponding to the coefficient $A^{[2]}(\omega)$ in the expansion (44), in which both fermion lines are Z-shaped (Fig. 3a). Formally, this reduces to replacing the two mass operators $\Sigma^e$ in (54) by their Z-like parts $\Sigma^{e(\mathrm{Z})}$ given by (55). As a result, after going over to the energy representation we obtain the following expression for the cancelling amplitude:

$$\begin{aligned}\Phi^{\mathrm{comp}}_{12,34}(\omega)=&\sigma_1\delta_{\sigma_1,-\sigma_2}\delta_{\sigma_3,-\delta_4}\delta_{\sigma_1,\sigma_3}\\&\times\int_{-\infty}^{\infty}\frac{d\varepsilon d\varepsilon'}{(2\pi i)^2}\xi_{12,34}(\omega,\varepsilon,\varepsilon')\Sigma^{e}_{31}(\varepsilon)\Sigma^{e}_{24}(\varepsilon'),\end{aligned} \tag{65}$$

where

$$\begin{aligned}\xi_{12,34}(\omega,\varepsilon,\varepsilon')=&\frac{1}{(\varepsilon-\tilde{\varepsilon}_1+i\sigma_1\delta)(\varepsilon'-\tilde{\varepsilon}_2-i\sigma_1\delta)(\varepsilon'-\tilde{\varepsilon}_4-i\sigma_1\delta)}\\&-\frac{1}{(\varepsilon-\tilde{\varepsilon}_1+i\sigma_1\delta)(\varepsilon-\tilde{\varepsilon}_3+i\sigma_1\delta)(\varepsilon'-\tilde{\varepsilon}_2-i\sigma_1\delta)}\\&+\frac{\omega'-\tilde{\varepsilon}_{12}+i\sigma_1\delta}{(\varepsilon-\tilde{\varepsilon}_1+i\sigma_1\delta)(\varepsilon-\tilde{\varepsilon}_3+i\sigma_1\delta)(\varepsilon'-\tilde{\varepsilon}_2-i\sigma_1\delta)(\varepsilon'-\tilde{\varepsilon}_4-i\sigma_1\delta)}.\end{aligned} \tag{66}$$

Equations (56)–(66), which uniquely determine the propagator $A(\omega)$ for known functions $\Sigma^e(\varepsilon)$ and $\mathscr{V}^e(\omega,\varepsilon,\varepsilon')$, do not contain integrals over the energy variables of the equations. This feature, important from the practical point of view, is a consequence of the separability of the $\varepsilon$ and $\varepsilon'$ dependences of the function $\widetilde{D}(\omega,\varepsilon,\varepsilon')$ discussed in the preceding section. This separability leads to the decoupling of the integrations over these variables in Eq. (48) after going to the energy representation [Eqs. (33)–(35)].

## 5. PROPERTIES OF THE PROPAGATOR OF THE TOGD METHOD IN VARIOUS MODELS

It follows from Eq. (21) for the response function and Eq. (25) for the strength function that in our approach the most important differences between the models describing nuclear structure amount to differences in the choice of specific approximation for the generalized $p-h$ propagator $A(\omega)$, because it is what determines all the types of dynamical effects included in a model. We shall consider two types of model, which are obtained by substituting specific expressions for the mass operator $\Sigma^e$ and the amplitude $\mathscr{V}^e$ into the general expressions of the TOGD method.

The substitution of Eqs. (14) and (15) for these quantities into Eqs. (60) and (65) leads to the model including $1p1h\otimes$phonon configurations within the TOGD method. The final expressions for the propagator $A(\omega)$ in this model are given in Ref. 18 (with two differences from the notation used here: $\Phi^{(2)}\equiv\widetilde{\Phi}$ and $\Phi^{(4)}\equiv\Phi^{\text{comp}}$). We note only that the expression for the amplitude $\Phi^{\text{comp}}(\omega)$ obtained from Eqs. (14), (65), and (66) differs from Eq. (24) of Ref. 18 for $\Phi^{(4)}(\omega)$ by the absence of pole terms. However, as already mentioned, this difference between $\Phi^{(4)}$ and $\Phi^{\text{comp}}$ only slightly affects the results of the calculations in this model owing to the smallness of $g^2$.

Let us consider the main features of the propagator of the TOGD method for the example of the model of Ref. 18.

### 5.1. The particle number conservation law

If the mass operator $\Sigma^e$ and the amplitude $\mathscr{V}^e$ are related by the identity (17) (as is true in the model of Ref. 18), from Eq. (60) we find

$$\sum_1 A^{[1]}_{11,34}(\omega)\equiv 0\equiv\sum_3 A^{[1]}_{12,33}(\omega). \tag{67}$$

This result is most easily obtained in the representation using wave functions of the basis set $\{\widetilde{\phi}_1,\widetilde{\varepsilon}_1\}$, in which, according to the definitions (11), we have

$$\widetilde{G}_1(\varepsilon+\omega)\widetilde{G}_1(\varepsilon)=\frac{1}{\omega}[\widetilde{G}_1(\varepsilon)-\widetilde{G}_1(\varepsilon+\omega)]. \tag{68}$$

In this case the identities (67) are proved by simple transformations using Eqs. (60), (17), (11), and (68). Since the unlike components of the propagator $A^{(--)}_{12,34}$ by definition do not have diagonal matrix elements in either the indices 1,2 or 3,4, from Eqs. (56)–(59) and (67) we obtain

$$\sum_1 A_{11,34}(\omega)\equiv 0\equiv\sum_3 A_{12,33}(\omega). \tag{69}$$

Furthermore, it follows from (21) that when (69) is satisfied analogous identities are valid for the renormalized response function $\widetilde{R}(\omega)$. If, in addition, the condition which must be satisfied by the parametrization of the effective charge operator

$$\sum_3 (\widetilde{e}_q)_{12,33}=c\,\delta_{12}$$

(where $c$ is a constant) does hold, then from Eq. (20) and the spectral expansion of the response function $R(\omega)$ (Ref. 15) we find that in the TOGD method we have

$$\sum_1 \langle n|a_1^+ a_1|0\rangle=0,\quad n\neq 0.$$

When the problem is solved exactly, these expressions are the simple consequence of the condition that the eigenfunctions of the ground and excited states be orthogonal together with the particle number conservation law. In the TOGD method, as in many other models, the validity of these fundamental conditions and laws is not *a priori* obvious, and the dynamical consistency condition (17) is essential for ensuring that they are satisfied. This implies that graphs containing self-energy insertions ($\Sigma^e$) and phonon lines in the "transverse" $p-h$ channel ($\mathscr{V}^e$) belong to the class of graphs associated with the particle number conservation law.[44] The consequent necessity of simultaneously including graphs of this type in models including $1p1h\otimes$phonon configurations is discussed in Refs. 14, 16, and 46.

Another important feature of the $p-h$ propagator of the TOGD method is that, in addition to the unlike components $A^{(--)}$, it also contains associated components: mixed $A^{(-+)}$,$A^{(+-)}$ and like $A^{(++)}$ components. The solution of Eq. (21) for $\widetilde{R}$ using this propagator also contains associated components, and therefore, in accordance with the spectral expansion of the response function, nonzero like components of the transition densities $\rho^{n0}_{pp'}$ and $\rho^{n0}_{hh'}$ appear, where $\rho^{n0}_{12}=\langle n|a_1^+ a_2|0\rangle$ (it is well known that in the RPA only the components $\rho^{n0}_{ph}$ and $\rho^{n0}_{hp}$ are nonzero). The appearance of the associated components of the $p-h$ propagator and the nonzero matrix elements $\rho^{n0}_{pp'}$ and $\rho^{n0}_{hh'}$ in the TOGD method is associated with the inclusion of ground-state correlations (GSCs) outside the framework of the RPA, which are discussed in Sec. 5 4. In what follows, in order to distinguish GSCs of this type from the GSCs which are included in the RPA, we shall use the notation GSC1 for the GSCs in the RPA and GSC2 for the GSCs outside the RPA.

We note that the addition of the associated components to the $p-h$ propagator when GSC2 are included requires a certain accuracy in the construction of the model, because it is here that the problem of whether or not Eqs. (69), associated with particle number conservation, can be satisfied becomes important (in models in which only the unlike components $A^{(--)}$ are nonzero, for example, the RPA and the SRPA, these equations are satisfied automatically).

### 5.2. The pole structure of the propagator in the TOGD method

Let us analyze the pole structure of the function $A(\omega)$. Specifically, we consider the question of the second-order poles, which is the technical problem the TOGD method is designed to solve. The fact that $A(\omega)$ does not contain second-order poles at the points $\omega=\pm(\tilde{\varepsilon}_p-\tilde{\varepsilon}_h)$, which are simple poles of the function $A^{[0]}(\omega)\equiv\tilde{A}(\omega)$, is almost obvious. Moreover, it follows from Eq. (61) that the function $A^{(--)}(\omega)$, and consequently also $A(\omega)$, is regular at these points if the matrix $\tilde{A}^{-1}(\omega)+\Phi(\omega)$ is invertible at these values of $\omega$ (a condition which can be violated only accidentally).

It is more difficult to answer the question of the behavior of the unlike components $A^{(--)}(\omega)$, and also of the mixed

$$A^{(-+)}(\omega)=A^{(--)}(\omega)Q^{(-+)}(\omega),$$

$$A^{(+-)}(\omega)=Q^{(+-)}(\omega)A^{(--)}(\omega),$$

and like

$$A^{(++)}(\omega)=Q^{(+-)}(\omega)A^{(--)}(\omega)Q^{(-+)}(\omega)+P^{(++)}(\omega) \tag{70}$$

components of the propagator at the poles of the functions $\tilde{\Phi}(\omega)$, $Q^{(-+)}(\omega)$, $Q^{(+-)}(\omega)$, and $P^{(++)}(\omega)$, which, according to Eqs. (57)–(59) and (64), coincide with the poles of the function $A^{[1]}(\omega)$. Equation (70) can also raise suspicion that in eliminating the second-order poles at the poles of the function $A^{[0]}(\omega)$ in the generalized $p-h$ propagator $A(\omega)$, the TOGD method leads to the appearance of other second-order poles in $A(\omega)$ which now coincide with the poles of the function $A^{[1]}(\omega)$. In the model where $1p1h\otimes$phonon configurations are included, the poles, discussed above, are located at the points $\omega=\Omega=\pm(\tilde{\varepsilon}_p-\tilde{\varepsilon}_h+\omega_m)$, where $\omega_m$ is the phonon energy. In order to formulate a statement about these poles, let us consider the decomposition of the function $A^{[1]}(\omega)$ near such a pole:

$$A^{[1]}_{12,34}(\omega)=\frac{a^{[1]\Omega}_{12,34}}{\omega-\Omega}+A^{[1]\Omega}_{12,34}(\omega),$$

where the function $A^{[1]\Omega}_{12,34}(\omega)$ is regular at the point $\omega=\Omega$. We shall assume that in the construction of the propagator $A(\omega)$ using (56)–(66) the one-particle basis $\{\tilde{\phi}_1,\tilde{\varepsilon}_1\}$ is restricted to a finite number of states of the discrete spectrum, as in all specific applications of the method. However, we shall assume that the size of this basis is arbitrary, so that the conclusions we make can be extended directly to the case of an infinite basis, including one containing the one-particle continuum. Introducing the multiple indices $i=\{1,2\}$, $j=\{3,4\}$, we find that in the restricted basis the residues of the function $A^{[1]}_{12,34}(\omega)$ at the pole $\omega=\Omega$ form a matrix $(a^{[1]\Omega}_{ij})$ of some finite rank. We use $(a^{[1]\Omega(--)}_{ij})$ to denote the block of this matrix of residues consisting of the unlike components of $a^{[1]\Omega}_{12,34}$, and $N^-_\Omega$ to denote the number of nonzero lines (or columns) of the matrix $(a^{[1]\Omega(--)}_{ij})$.

We can make the following statement allowing the behavior of the TOGD propagator $A(\omega)$ to be determined at the point $\omega=\Omega$, which is a pole of at least one of the functions $\tilde{\Phi}(\omega)$, $Q^{(-+)}(\omega)$, $Q^{(+-)}(\omega)$, and $P^{(++)}(\omega)$:

(1) When certain sufficiently general conditions are satisfied, the unlike $A^{(--)}(\omega)$ and mixed $A^{(-+)}(\omega)$, $A^{(+-)}\times(\omega)$ components of the TOGD propagator are regular at the point $\omega=\Omega$, and for the like components $A^{(++)}(\omega)$ the point $\omega=\Omega$ is either a simple pole or a removable singularity;

(2) If, in addition, the condition

$$\text{rank}\ (a^{[1]\Omega}_{ij})\geq N^-_\Omega \tag{71}$$

is satisfied, the function $A^{(++)}_{12,34}(\omega)$ is regular at the point $\omega=\Omega$.

The rigorous proof of this statement with the exact formulation of the general conditions contained in it (associated with the invertibility of specially defined matrices) is not given here because its full treatment would take a great deal of space and is a purely mathematical problem. In specific applications of the TOGD method the general conditions of this statement can apparently be violated only accidentally. The situation regarding the condition (71) is different, because the quantities involved in it have an essential dependence on the characteristics of the pole at the point $\omega=\Omega$ and the dimension of the one-particle basis $\{\tilde{\phi}_1,\tilde{\varepsilon}_1\}$. In particular, it is always violated if the propagator has no nonzero unlike components at all, so that $N^-_\Omega=0$. In this case, $A(\omega)=A^{(++)}(\omega)=P^{(++)}(\omega)$. This situation can arise, for example, in calculations using a greatly restricted basis, if $p-h$ transitions are absent from it owing to selection rules.

Let us see in which cases the condition (71) will be satisfied. If the nucleus has spherical symmetry, it can be shown that for the model of Ref. 18, the rank of the matrix of residues of the function $A^{[1]}(\omega)$ at its pole $\omega=\Omega=\pm(\tilde{\varepsilon}_p-\tilde{\varepsilon}_h+\omega_m)$ satisfies the inequality

$$\text{rank}\ (a^{[1]\Omega}_{ij})\leq\Lambda_\Omega, \tag{72}$$

where $\Lambda_\Omega$ is equal to the number of integer values of $l$ satisfying two conditions:

$$|j_p-j_h|\leq l\leq j_p+j_h,\quad |J-L_m|\leq l\leq J+L_m.$$

Here $j_p$ and $j_h$ are the angular momenta of one-particle states with energies $\tilde{\varepsilon}_p$ and $\tilde{\varepsilon}_h$, $L_m$ is the angular momentum of the phonon with energy $\omega_m$, and $J$ is the angular momentum of the excitations under study [i.e., of the external field $V^0$ in (1)]. Therefore, in this model, the quantity $\text{rank}(a^{[1]\Omega}_{ij})$, which can be termed the degree of degeneracy of the pole, is bounded from above by the number $\Lambda_\Omega$, which is determined only by the characteristics of the pole at the point $\omega=\Omega$ and the angular momentum $J$ and is independent of the size of the one-particle basis $\{\tilde{\phi}_1,\tilde{\varepsilon}_1\}$ (of course, if states with energies $\tilde{\varepsilon}_p$ and $\tilde{\varepsilon}_h$ enter into this basis). On the other hand, the number $N^-_\Omega$ in the inequality (71) grows as the size of the one-particle basis increases, and for any pole of the function $A^{[1]}(\omega)$ at a point $\omega=\Omega$ there is a basis $\{\phi_1,\tilde{\varepsilon}_1\}$ for which (and for any other basis containing this basis as a subset) $N^-_\Omega\geq\Lambda_\Omega$. Owing to (72), we find that the condition (71) in this case is satisfied, and so all the components of the propagator $A(\omega)$ are regular at the point $\omega=\Omega$.

This implies that in the solution of the problem of constructing the TOGD $p-h$ propagator in the complete one-particle basis, all its components are regular at singular points of the function $A^{[1]}(\omega)$. Here each singular point of the associated components of $A(\omega)$ is simultaneously a singular point of the unlike component $A^{(--)}(\omega)$. In other words, when the full one-particle basis $\{\tilde{\phi}_1, \tilde{\varepsilon}_1\}$ is used, all the poles of the propagator $A(\omega)$ coincide with the poles of its unlike component $A^{(--)}(\omega)$. We have studied the poles of the function $A(\omega)$ in such great detail only to justify this statement, because, as we shall see below, it is closely related to the problem of including the GSC2.

The analysis of the poles of the function $A^{(--)}(\omega)$ itself is a different, independent problem, and we shall not discuss it here. We restrict ourselves to the remark that all its poles are shifted relative to those of the functions $\tilde{A}(\omega)$ and $\Phi(\omega)$ involved in (61). Moreover, the number of poles of $A^{--}(\omega)$ can be greater than the total number of poles of the functions $\tilde{A}(\omega)$ and $\Phi(\omega)$ owing to the splitting of the poles of $\Phi(\omega)$ in the complete or partial lifting of their degeneracy in the solution of (61). These effects of shifting and splitting of poles are of order $g^2$.

Let us point out yet another role of the term $Q^{(+-)} \times(\omega)A^{(--)}(\omega)Q^{(-+)}(\omega)$ on the right-hand side of (70) for the like component of the TOGD $p-h$ propagator. Although formally in the model including $1p1h\otimes$phonon configurations this term is of order $g^4$, in satisfying the corresponding conditions it is it which ensures the removal of the singularities of the component $A^{(++)}(\omega)$ which coincide with the poles of the function $P^{(++)}(\omega)=A^{[1](++)}(\omega)$ [the pole of the function $A^{(++)}(\omega)$ at the point $\omega=\Omega$ is eliminated when the residues of the two terms on the right-hand side of (70) become equal in magnitude and opposite in sign]. This term contains the poles of $A^{(++)}(\omega)$ which coincide with the poles of the unlike component $A^{(--)}(\omega)$. The fact that its inclusion causes the propagator $A(\omega)$, when constructed rigorously, to have no "extra" poles serves as indirect confirmation of the correctness of the model approximations of the TOGD method.

### 5.3. Models including "pure" $2p2h$ configurations

Let us now turn to models of the SRPA type, which are obtained when Eqs. (12) and (13) for $\Sigma^e$ and $\mathscr{H}^e$ are substituted into (60) and (65). Since a different mathematical apparatus is usually used in constructing models of this type, comparison of the results of our approach with the known expressions of Ref. 2 requires additional transformations. The SRPA scheme with uncorrelated $2p2h$ states is equivalent to the inclusion of only the unlike components of the generalized TOGD $p-h$ propagator $A^{(--)}$. The contributions of GSC2 effects are eliminated from the other components. Formally, this implies that $\Phi=\tilde{\Phi}$ in Eq. (61) for $A^{(--)}$, while in Eqs. (64) and (60) determining $\tilde{\Phi}$ the Z-like parts (55) are excluded from the mass operators $\Sigma^e$ [Eq. (12)], and only the matrix elements of the amplitude $\mathscr{H}^e$ [Eq. (13)] of the form $\mathscr{H}^e_{ph,p'h'}$, $\mathscr{H}^e_{hp,h'p'}$ are included. Moreover, the effective $p-h$ interaction amplitude in Eq. (21) for the response function is assumed to be equal to the two-particle interaction amplitude entering into (12) and (13): $\tilde{\mathscr{F}}_{12,34}=w_{23,14}$, and the mass operator $\tilde{\Sigma}$ is determined in the Hartree–Fock approximation.

We see that GCS2 effects are not taken into account at all in this model. If no additional transformations are made after substituting Eqs. (12) and (13) into (60) and (65), so that all the components of the generalized TOGD $p-h$ propagator are preserved, we obtain a model comparable to the extended second RPA (the ESRPA; Ref. 2). It follows from the logic of constructing the model that GSC2 effects are taken into account in it completely in terms of second order in the interaction amplitude $w$ and partially in terms of higher order in this amplitude (there is no GSC2 contribution to the response function in zeroth and first orders in $w$). However, the detailed comparison of this model and the ESRPA is nontrivial, and we shall not dwell on it here. The general theoretical foundation of models of this class, which in our approach amounts to justification of the approximations (12) and (13) for $\Sigma^e$ and $\mathscr{H}^e$, has been discussed briefly in Sec. 2.

We stress the fact that all the properties of the generalized TOGD $p-h$ propagator studied in this section, including the particle number conservation law, remain valid also for the ESRPA-type model obtained in our approach. The only formal difference is that in this case the poles of the functions $\tilde{\Phi}(\omega)$, $Q^{(-+)}(\omega)$, $Q^{(+-)}(\omega)$, and $P^{(++)}(\omega)$ discussed above will be located at the points $\omega=\Omega=\pm(\tilde{\varepsilon}_p-\tilde{\varepsilon}_h+\tilde{\varepsilon}_{p'}-\tilde{\varepsilon}_{h'})$.

### 5.4. Effects of ground-state correlations and their relation to the pole structure of the TOGD propagator

Here we shall consider only the effects of ground-state correlations, the contributions of which are absent in the ordinary RPA, i.e., GSC2 effects. In recent years, the interest in studying the influence of these effects on nuclear properties has prompted studies in which their contribution is analyzed in calculations of the excitation spectra of specific nuclei (Refs. 10, 16, 31–33 and 45. It has been shown that GSC2 effects play an important, sometimes decisive, role in the theoretical description of the experimental data (see also Sec. VI below).

There is a fundamental difference between the effects of ground-state correlations in the RPA and their effects in models where complex $(2p2h)$ configurations are included. As is well known, the inclusion of GSC in the RPA, which is the difference between the Tamm–Dankov approximation (TDA) and the RPA, does not lead to the appearance of new states compared to the TDA, but only shifts the energies of the TDA levels and redistributes their intensity. In the terminology of the Green function formalism, this means that the number of poles of the response function $\tilde{R}(\omega)$ in the region Re $\omega>0$ is the same in the TDA and the RPA.

In our approach GSC2 effects can be split into two categories: regular and singular. Regular effects are those whose inclusion does not change the number of poles of the generalized $p-h$ propagator $A(\omega)$, but affects only their location and the value of their residues. In the model of Ref. 18 the processes due to these effects correspond to Z-graphs

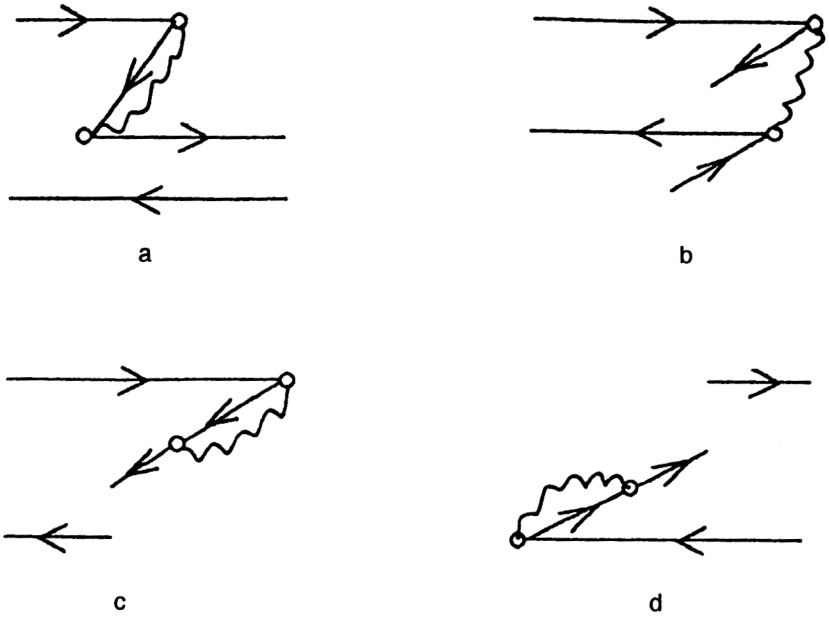


FIG. 4. Typical graphs of order $g^2$ due to regular effects of ground-state correlations. The notation is the same as in Fig. 2.

with self-energy insertions (Fig. 4a), graphs with a phonon line in the "transverse" $p-h$ channel similar to those shown in Fig. 4b, and some other backward-running graphs with self-energy insertions (Figs. 4c and 4d). In Fig. 4 we show only the typical time-ordered graphs of second order in the quasiparticle–phonon interaction amplitude. The graphs of Figs. 4a and 4b correspond to contributions to $A^{(--)}$, the graph of Fig. 4c corresponds to contributions to $A^{(-+)}$, and the graph of Fig. 4d corresponds contributions to $A^{(+-)}$.

It should be noted that the GSC2 effects included in the model of Ref. 45 can in our classification be associated with regular effects, although in that model, which also includes nucleon pair correlations, it would be more accurate to refer to them as regular GSC effects outside the QRPA.

Effects whose inclusion can lead to the appearance of new (additional) poles in the function $A(\omega)$ will be called singular GSC2 effects. Typical graphs of order $g^2$ arising from these effects are shown in Fig. 5. The graph of Fig. 5a corresponds to contributions to $A^{(-+)}$, the graph of Fig. 5b corresponds to contributions to $A^{(+-)}$, and the graphs of Figs. 5c and 5d correspond to contributions to $A^{(++)}$. All of these graphs, like those of Fig. 4, are classified as backward-running graphs, where the ones of Figs. 5a and 5c contain self-energy insertions, while those in Figs. 5b and 5d contain phonon lines in the "transverse" $p-h$ channel.

The concept of new poles of the propagator $A(\omega)$ in these definitions should be made more precise. Here by new poles of $A(\omega)$ we mean poles which are absent in the RPA propagator $\tilde{A}(\omega)$ (62) and cannot be obtained from the poles of this function by any continuous transformation (for example, by shifting the poles of $\tilde{A}(\omega)$ as $g^2$ increases from zero to some finite value). It is these new poles, which we shall refer to as new poles of the first type, which serve as the

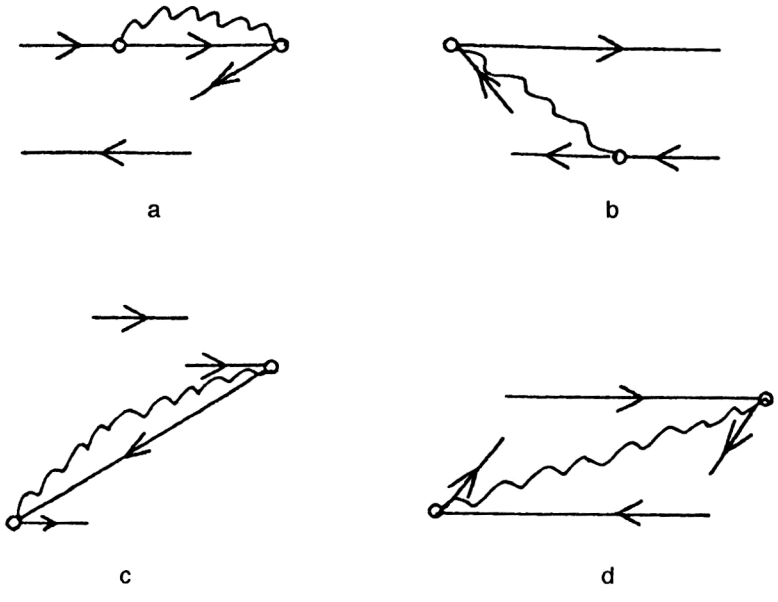


FIG. 5. Typical graphs of order $g^2$ due to singular effects of ground-state correlations. The notation is the same as in Fig. 2.

criterion for our division of GSC2 effects into regular and singular. We note that singular GSC2 effects contribute only to the associated components of the TOGD propagator, and these components themselves exist exclusively owing to GSC2 effects.

Let us consider a question which is important from the practical point of view: when singular GSC2 effects are included, is it possible for new poles of $A(\omega)$ to appear which are not present either in the RPA propagator $\widetilde{A}(\omega)$ or in the TOGD propagator, from which all contributions of GSC2 effects are excluded? Since only the unlike components of the generalized $p-h$ propagator remain when GSC2 effects are excluded, here we are speaking of poles of the function $A^{(--)}(\omega)$. It follows from the analysis of the preceding section that the appearance of new poles of this, the second, type is actually possible only when the condition (71) is violated (this can occur only when a restricted basis $\{\widetilde{\phi}_1,\widetilde{\varepsilon}_1\}$ is used) and only for the like component $A^{(++)}\times(\omega)$, because the mixed components of the propagator $A^{(-+)}(\omega)$ and $A^{(+-)}(\omega)$ can have poles at only the locations of the poles of the function $A^{(--)}(\omega)$ (as mentioned above, the poles of $A^{(--)}(\omega)$ are shifted relative to the "bare" poles of the functions $\widetilde{A}(\omega)$ and $\Phi(\omega)$ entering into $A^{(--)}(\omega)$, and their number can exceed the number of these bare poles). Since specific applications of the TOGD use a restricted basis for calculating the associated components of $A(\omega)$, the inclusion of singular GSC2 effects can in some cases enrich the pole spectrum of the generalized p-h propagator, and, consequently, of the response function $\widetilde{R}(\omega)$, and can lead to a change of the nuclear excitation spectrum relative to the TOGD case including GSC2 effects. Therefore, in constructing the TOGD propagator we shall need to analyze the effect of the size of the one-particle basis.

Another special feature of singular GSC2 effects is the fact that their inclusion leads to the appearance of nonzero matrix elements of the transition densities $\rho^{no}_{pp'}$ and $\rho^{no}_{hh'}$. From the physical point of view, the graphs due to this type of GSC2 (Fig. 5) describe processes of creation from the vacuum, which is the ground state of the even–even nucleus in question, and (or) the simultaneous annihilation of two $p-h$ pairs, i.e., $2p2h$ configurations. In this case the action of the external field $V^0$ leads to a transition, allowed by the selection rules, of the particle involved in the $2p2h$ configuration from one state to another (a $p-p'$ transition) or of the hole in this configuration to another hole state (an $h-h'$ transition). Formally, this implies that the spectral expansion of the response function now contains components of the transition densities such as $\rho^{no}_{pp'},\rho^{no}_{hh'}$, in addition to the usual $(\rho^{no}_{ph},\rho^{no}_{hp})$ components. The inclusion of these effects leads in particular to a change of the sum rules for the moments of the strength function. This has been discussed in Refs. 2 and 11 for the case of "pure" $2p2h$ configurations, i.e., the ES-RPA. Our results obtained using the model including $1p1h\otimes$phonon configurations have shown the importance of the quantitative inclusion of singular GSC2 effects (see Sec. 6).

We already see from this brief discussion of GSC2 effects that they are manifested in a considerably more complicated way than GSC1 effects. Therefore, this question merits further study.

## 6. ANALYSIS OF GMR USING THE TOGD METHOD INCLUDING THE ONE-PARTICLE CONTINUUM

### 6.1. Inclusion of the one-particle continuum in the coordinate representation

In calculations of the GMR strength functions it is useful to go from the Bethe–Salpeter equation (21) for the renormalized response function $\widetilde{R}$ to the equation for the change of the density matrix $\delta\rho$, given by

$$\delta\rho_{12}(\omega)=-\sum_{34}\widetilde{R}_{12,34}(\omega)(\widetilde{e}_qV^0)_{43}.$$

In the coordinate representation the equation for this quantity is (for simplicity, here and below we drop the spin–isospin variables)

$$\delta\rho(\mathbf{r};\omega)=-\int d\mathbf{r}_1A(\mathbf{r},\mathbf{r}_1;\omega)\widetilde{e}_qV^0(\mathbf{r}_1)$$
$$-\int d\mathbf{r}_1d\mathbf{r}_2A(\mathbf{r},\mathbf{r}_1;\omega)\widetilde{\mathcal{F}}(\mathbf{r}_1,\mathbf{r}_2)\delta\rho(\mathbf{r}_2;\omega). \tag{73}$$

The strength function (25) is related to $\delta\rho$ as

$$S(E,\Delta)=-\frac{1}{\pi}\,\mathrm{Im}\int d\mathbf{r}(\widetilde{e}_qV^0(\mathbf{r}))^*\delta\rho(\mathbf{r};E+i\Delta). \tag{74}$$

The use of the coordinate representation allows the propagator to be constructed by the efficient method of calculating the one-particle Green function $\widetilde{G}(\mathbf{r},\mathbf{r}_1;\omega)$ with the exact inclusion of the one-particle continuum.[4,5] The effects associated with resonance decay into the continuum (the width $\Gamma\uparrow$), i.e., with nucleon emission from the nucleus, are thereby "automatically" included in the strength function calculated using Eqs. (73) and (74).

The systematic use of this technique, which was first developed in the RPA, for the problem of the additional inclusion of $1p1h\otimes$phonon configurations leads to great computational difficulties in the construction of the generalized propagator $A$.[6] Therefore, at this stage of the investigations we included the continuum exactly only in the $1p1h$ part of the propagator using the idea of the combined $(\mathbf{r},\lambda)$ representation developed within the "finite Fermi system + continuum" approach for nuclei with pairing.[47] In this approximation the complete propagator is written as

$$A(\mathbf{r},\mathbf{r}_1;\omega)=\widetilde{A}^{\mathrm{cont}}(\mathbf{r},\mathbf{r}_1;\omega)+\sum_{1234}(A_{12,34}(\omega)$$
$$-\widetilde{A}_{12,34}(\omega))\widetilde{\phi}^*_1(\mathbf{r})\widetilde{\phi}_2(\mathbf{r})\widetilde{\phi}_3(\mathbf{r}_1)\widetilde{\phi}^*_4(\mathbf{r}_1). \tag{75}$$

Here $\widetilde{A}^{\mathrm{cont}}$ is the $1p1h$ propagator [Eq. (62)] in which the one-particle continuum is included exactly.[4,5] The summation runs over all one-particle discrete and quasidiscrete states included in the restricted set $\{\widetilde{\phi}_1,\widetilde{\varepsilon}_1\}$. The following section is devoted to the construction of this basis set. The

subtraction of $\tilde{A}_{12,34}$ eliminates double counting of the discrete $1p1h$ part of the propagator entering into both $\tilde{A}^{\rm cont}$ and $A_{12,34}$.

### 6.2. Construction of the basis $\{\tilde{\phi}_1, \tilde{\varepsilon}_1\}$

In the Dyson equation for the one-particle Green function (5), the complete mass operator $\Sigma$ includes all possible effects of the coupling of one- and multiparticle degrees of freedom of the nucleus leading to observable characteristics of the "one-particle" motion in odd nuclei (the energies, spectroscopic factors, and so on). If we start from the condition that these characteristics are reproduced best in an approach not including complex configurations, then in the construction of the phenomenological basis $\{\tilde{\phi}_1, \tilde{\varepsilon}_1\}$ the operator $\Sigma$ is replaced by its quasiparticle part $\Sigma_q$ (Ref. 35), and then the basis found by solving Eq. (5) with $\Sigma = \Sigma_q$ is used in $1p1h$ calculations for even–even nuclei. The contribution of the quasiparticle–phonon interaction is explicitly isolated in the TOGD method, because in this case, if the corresponding corrections are not introduced (i.e., if the basis is not "refined"), the use of the phenomenological basis can lead to double counting of these effects.

The basis $\{\tilde{\phi}_1, \tilde{\varepsilon}_1\}$ including these corrections is constructed in our model starting from the condition that the "dominant" poles of the solution of Eq. (7) (i.e., the poles of the Green function $G$ with maximum values of the residues) coincide with the experimental one-particle energies $\varepsilon_1^{\rm exp}$. In the calculations we use the basis including the two shells below and the two shells above the Fermi energy. In the diagonal approximation for $\Sigma_{12}^e$ the above condition leads to the following system of nonlinear equations:

$$\tilde{\varepsilon}_1 = \varepsilon_1^{\rm exp} - \sum_{3,m} \frac{|g_{13}^{m(\sigma_3)}|^2}{\varepsilon_1^{\rm exp} - \tilde{\varepsilon}_3 - \sigma_3 \omega_m}. \tag{76}$$

This system, supplemented by Eq. (6) for the Green function $\tilde{G}$, is solved iteratively, with the mass operator $\tilde{\Sigma}$ in (6) approximated by the Woods–Saxon potential. Since $g^2$ is a small parameter, when solving this problem we can limit ourselves to the first iteration. In this approximation the matrix elements $g_{13}^{m(\sigma_3)}$ in Eq. (76) are calculated using the wave functions of the phenomenological basis, obtained by solving the Schrödinger equation with the Woods–Saxon potential parameterized by an emiprical set of constants. Here the energies $\tilde{\varepsilon}_1$ are found directly by solving the system (76), and the depth parameters of the potential $\tilde{\mathcal{U}}$,[7] approximating the mass operator $\tilde{\Sigma}$ are chosen from the condition that the poles of the solution of (6) (i.e., the Green function $\tilde{G}$) coincide with the values found for $\tilde{\varepsilon}_1$. Finally, the wave functions $\tilde{\phi}_1$ are determined by solving the Schrödinger equation with the potential $\tilde{\mathcal{U}}$.

### 6.3. Additional details of the calculations

In our calculations we included a limited number of the most strongly collectivized, low-lying phonons of normal parity: $2^+$, $3^-$, $4^+$, and $6^+$. Their parameters, the energies $\omega_L$ and transition probabilities $B(EL)$, are given in Refs. 29, 30, and 31 for all the nuclei studied.

The effective Landau–Migdal $p-h$ interaction[35]

$$\mathcal{F}(\mathbf{r},\mathbf{r}') = C_0[f(r) + f'(r)\boldsymbol{\tau}_1\boldsymbol{\tau}_2 + (g + g'\boldsymbol{\tau}_1\boldsymbol{\tau}_2)\boldsymbol{\sigma}_1\boldsymbol{\sigma}_2]\delta(\mathbf{r} - \mathbf{r}') \tag{77}$$

was used in all the calculations, with the density-dependent parameters $f$ and $f'$: $f = f_{ex} + (f_{in} - f_{ex})\rho(r)/\rho(0)$ and similarly for $f'$. With the exception of the parameter $f_{ex}$, practically all the calculations used the same set of parameters found from self-consistent calculations using the theory of finite Fermi systems:[49,50]

$$f_{\rm in} = -0.002, \quad f'_{\rm ex} = 2.30, \quad f'_{\rm in} = 0.76$$

$$g = -0.05, \quad g' = 0.96, \quad C_0 = 300 \ \text{MeV}\cdot\text{fm}^3. \tag{78}$$

The calculations of the $M1$ resonance in stable and unstable magic nuclei were performed using the parameters $g = -0.05$ and $g' = 0.86$, for which good agreement was obtained between the calculated and experimental values of the resonance energies in the $^{48}$Ca nucleus. We used the parameter $f_{ex} = -3.74$ in order to eliminate the isoscalar "ghost" $E1$ state in the calculations of the isovector $E1$ resonance. In the calculations of the isoscalar $E0$ resonance[32] the parameter $f_{ex} = -3.00$ was chosen from the experimental location of the resonance in the $^{208}$Pb nucleus. To make the theoretical and experimental values of the energies of low-lying isosclar phonons agree, $f_{ex}$ was taken from the range of $f_{ex}$ from $-3.50$ to $-5.00$.

The interpolation function $\rho(r)$ in (77) was taken to be the Woods–Saxon form factor:

$$\rho(r) = \frac{\rho_0}{1 + \exp((r-R)/a)},$$

$$R = 1.24A^{1/3}, \quad a = 0.63. \tag{79}$$

Our recent calculations of the isoscalar $E0$ and $E2$ resonances in $^{40}$Ca (Ref. 33) and $^{56}$Ni are exceptions; here for $\rho(r)$ we used the calculated density in the nuclear ground state:

$$\rho(r) = \sum_{\tilde{\varepsilon}_i \le \varepsilon_F} \frac{(2j_i+1)\tilde{\phi}_i^2(r)}{4\pi}. \tag{80}$$

This introduced an element of consistency into our non-self-consistent calculations with independently chosen mean-field and effective $p-h$ interaction parameters.

The explicit inclusion of quasiparticle–phonon correlations in the TOGD method leads to renormalization of the effective interaction $\tilde{\mathcal{F}}$ and the effective charges $\tilde{e}_q$ [see Eqs. (22)–(24)], which differ from $\mathcal{F}$ and $e_q$ used in the theory of finite Fermi systems. However, since a relatively small number (no more than ten) of phonons were used in the calculations, the difference of $\tilde{\mathcal{F}}$ and $\tilde{e}_q$ from $\mathcal{F}$ and $e_q$ should not be important. In connection with this and to avoid introducing additional parameters to take into account these differences, in all the RPA and TOGD calculations we used the same interaction $\tilde{\mathcal{F}} = \mathcal{F}$ and effective charges $\tilde{e}_q = e_q$.

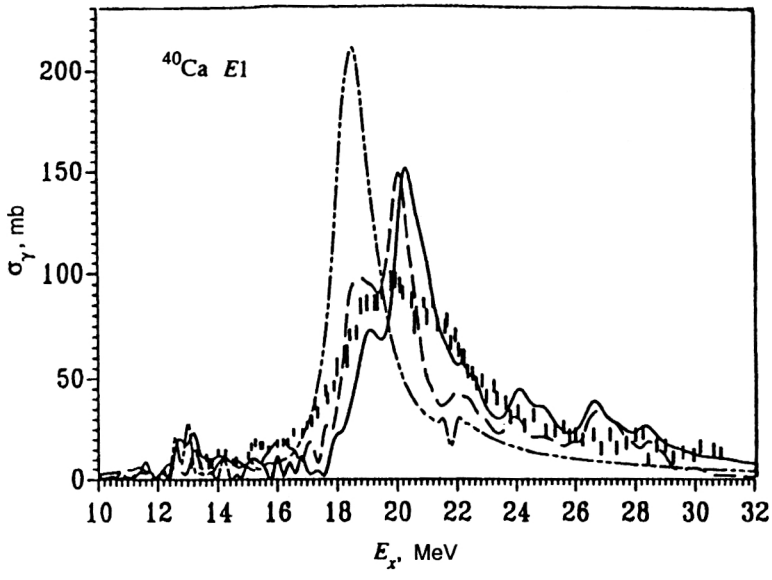


FIG. 6. $E1$-photoabsorption cross section for $^{40}$Ca. The dot–dash line is the RPA+continuum calculation, and the dashed and solid lines are the TOGD calculations respectively neglecting and including the continuum (GSC2 effects are included). The experimental data are taken from Ref. 51.

To mimic the experimental energy resolution and at the same time phenomenologicaly include effects not dealt with explicitly in the TOGD method (further GMR fragmentation due to configurations more complex than $2p2h$, and decay of complex configurations into the continuum, leading to the additional width $\Gamma\uparrow$), in the calculations of the strength functions we used the smoothing parameter $\Delta=\Gamma/2$ ($\Gamma$ is the width of the Breit–Wigner distribution for an isolated peak of the strength function) from the range $\Delta=100-500$ keV. When studying the fine structure of resonances, for example, for the isoscalar $E2$ resonance in $^{208}$Pb (Ref. 31), we used the parameter $\Delta=20$ keV.

### 6.4. Results of the calculations

Our main goal in this review is to describe the foundations of the TOGD method as a new approach for studying the structure of magic nuclei with the systematic inclusion of quasiparticle–phonon correlations in the ground and excited states and with the additional inclusion of the one-particle continuum. The calculated results given below and their discussion for isoscalar and isovector $EL$ and $M1$ resonances in the stable $^{40,48}$Ca, $^{208}$Pb and unstable $^{56}$Ni, $^{100}$Sn magic nuclei are incomplete. A more complete discussion can be found in the original studies (Refs. 17, and 27–34).

The notation $2p2h(gs+)$ and $2p2h(gs-)$ encountered in the figures refers to the TOGD calculations performed respectively including and neglecting GSC2 effects (i.e., $1p1h\otimes$phonon correlations in the ground state). By definition, neglect of GCS2 effects means that the functions $Q^{(+-)}$, $Q^{(-+)}$, and $P^{(++)}$ in the full propagator $A(\omega)$ (56) are equal to zero. When GSC2 effects are included, the basis is always chosen such that the case $A(\omega)=A^{(++)}\times(\omega)=P^{(++)}(\omega)$ is practically never realized. The results of the TOGD calculations given in Figs. 6 and 7 were obtained taking into account these correlations. In order to demonstrate the effect of the one-particle continuum on the shape of the curve for the photoabsorption cross section and on the integrated characteristics of the $E1$ resonance, in these

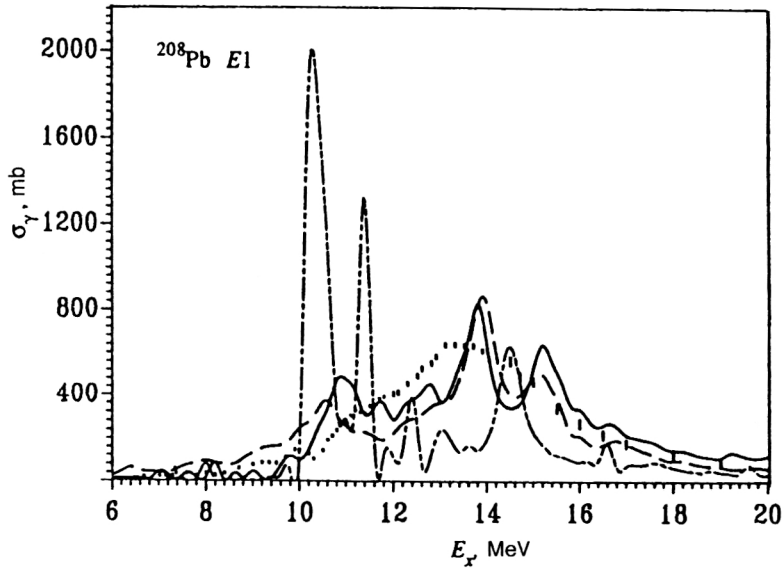


FIG. 7. The same as in Fig. 1, but for $^{208}$Pb. The experimental data are taken from Ref. 53.

TABLE I. Integrated characteristics of the isovector $E1$ resonance. GSC2 correlation effects have been included in the TOGD calculations for $^{40,48}$Ca and $^{208}$Pb. All the calculations for $^{56}$Ni include the continuum. $\bar{E}$, $\Delta E$, and $\Gamma$ are given in MeV, $\sigma_{max}$, and $\sigma_{-1}$ in mb, and $\sigma_0$ and $\sigma_0^{cl}$ in mb·MeV.

| | $\sigma_{max}$ | $\bar{E}$, MeV | $\Gamma$ | $\sigma_0$, mb·MeV | $\sigma_{-1}$, mb |
|---|---|---|---|---|---|
| | | $^{40}$Ca, $\sigma_0^{cl}=600$, | $\Delta E=(10-32)$ | | |
| RPA (cont+) | 210.0 | 19.3 | 1.9 | 586.3 | 30.26 |
| TOGD(cont−) | 114.0 | 20.5 | 3.7 | 589.7 | 28.83 |
| TOGD(cont+) | 111.0 | 21.2 | 4.3 | 651.8 | 30.89 |
| Experiment (Ref. 51) | 95.0 | 20.0 | 5.0 | 637.7 | 31.82 |
| | | $^{48}$Ca, $\sigma_0^{cl}=700$, | $\Delta E=(10-32)$ | | |
| RPA (cont+) | 150.0 | 16.0 | 3.3 | 652.5 | 42.66 |
| TOGD(cont−) | 118.7 | 19.0 | 4.5 | 696.9 | 38.34 |
| TOGD(cont+) | 101.3 | 19.6 | 6.3 | 756.5 | 41.60 |
| Experiment (Ref. 52) | 102.7 | 19.6 | 7.1 | 836.6 | 43.37 |
| | | $^{208}$Pb, $\sigma_0^{cl}=2980$, | $\Delta E=(6-20)$ | | |
| RPA (cont+) | 945.0 | 12.2 | 2.0 | 2709.0 | 222.60 |
| TOGD(cont−) | 657.0 | 13.0 | 3.6 | 3110.0 | 243.70 |
| TOGD(cont+) | 680.0 | 13.8 | 3.9 | 3367.0 | 251.50 |
| Experiment (Ref. 53) | 640.0 | 13.42 | 4.05 | 3306.8 | 253.77 |
| | | $^{56}$Ni, $\sigma_0^{cl}=840$, | $\Delta E=(5-30)$ | | |
| RPA | 211.0 | 18.5 | 3.1 | 873.4 | 44.83 |
| TOGD | 170.0 | 18.7 | 4.0 | 908.2 | 46.12 |
| TOGD(GSC2) | 140.0 | 18.2 | 4.9 | 916.0 | 47.80 |

figures and in Table I we also give the results of the TOGD calculations neglecting the continuum (labeled "cont−"). For the $E1$ resonance in $^{56}$Ni and for all the other E$L$ and $M1$ resonances we show only the results of the calculations taking into account the continuum ("cont+").

*Isovector $E1$ and $E2$ resonances in the nuclei* $^{40,48}$Ca, $^{208}$Pb, *and* $^{56}$Ni. The cross sections for dipole and quadrupole photoabsorption were calculated using the well known equation

$$\sigma_{EL}(E,\Delta)=\frac{8\pi^3(L+1)e^2}{L[(2L+1)!!]^2}\left(\frac{E}{\hbar c}\right)^{2L-1}S_{EL}(E,\Delta). \quad (81)$$

We give the results of these calculations in Figs. 6–8 and in Tables I and II (Refs. 17, 29, and 31). For obtaining the integrated characteristics of the resonances we used the Lorentz function to approximate the resonance curves

$$\sigma^L(E)=\sigma_{max}\frac{E^2\Gamma^2}{(E^2-\bar{E}^2)^2+E^2\Gamma^2},$$

as is commonly done in analyzing experiments. The parameters of this function, the average energy $\bar{E}$, the cross section $\sigma_{max}=\sigma^L(\bar{E})$, and the resonance width $\Gamma$, are found from the condition that the three energy moments with $k=0$, 1, and 2 coincide for the exact and approximating resonance curves. These moments were calculated from the expression

$$\sigma_k=\int_{E_{min}}^{E_{max}}E^k\sigma(E)dE.$$

The energy ranges $\Delta E=(E_{min}-E_{max})$ are given in Tables I and II, which gives the integrated photoabsorption cross sec-

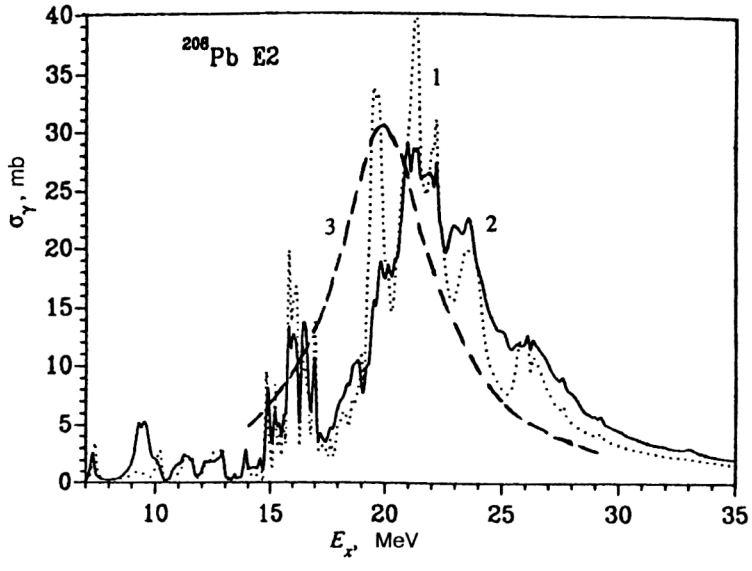


FIG. 8. Cross section for $E2$ photoabsorption for $^{208}$Pb calculated in the RPA (curve 1) and the TOGD taking into account the continuum (curve 2) (GSC2 effects are not included). The experimental data (curve 3) are taken from Ref. 56.

TABLE II. Integrated characteristics of the isovector $E2$ resonance. GSC2 correlation effects are not included in the TOGD calculations. $\bar{E}$, $\Delta E$, and $\Gamma$ are given in MeV, $\sigma_{max}$, and $\sigma_{-1}$ in mb, and $\sigma_0$ and $\sigma_0^{cl}$ in mb·MeV.

| | $^{40}$Ca $\Delta E=(10-50)$ | | | $^{208}$Pb, $\Delta E=(17.5-35)$ | | | |
|---|---|---|---|---|---|---|---|
| | $\bar{E}$ | $\Gamma$ | $\sigma_0$ | $\sigma_{max}$ | $\bar{E}$ | $\Gamma$ | $\sigma_0$ |
| RPA(cont+) | 32.8 | 8.5 | 37.7 | 31.6 | 21.9 | 4.5 | 183.0 |
| TOGD(cont+) | 31.8 | 7.0 | 32.0 | 28.1 | 22.4 | 5.5 | 192.1 |
| Experiment | 32.5 ± 1.5(a) | | | 31.0 | 20.2 ± 0.5 | 5.5±0.5 | 203.0(b) |
| | | | | | 22.6 ± 0.4 | 6.0±2.0(c) | |
| | | | | | 23.5 ± 1.5(d) | | |

The experimental data are taken from Refs. 55(a), 56(b), 57(c), and 58(d).

tions $\sigma_0$ and moments $\sigma_{-1}$ (for the $E1$ resonance). For the $E1$ resonance $\sigma_0$ is compared to the "classical" Thomas–Reiche–Kuhn dipole sum rule:

$$\sigma_0^{cl}=\int_0^{\infty}\sigma_{E1}(E)dE=60\frac{NZ}{A}\ (\text{mb}\cdot\text{MeV}). \tag{82}$$

Comparison of the calculation and experiment and analysis of our results led to the following conclusions for $E1$ resonances:

•The RPA calculations taking into account the continuum agree poorly with experiment for all the nuclei studied. The only exception is the result for the centroid $\bar{E}$ of the resonance in $^{40}$Ca and the moments $\sigma_{-1}$ in $^{40,48}$Ca.

•The inclusion of complex $1p1h\otimes$phonon configurations and the one-particle continuum significantly improves the description of the resonance shape and all the observed integral characteristics of the resonance.

•As seen from Table I, the inclusion of GSC2 effects has a fairly weak influence on the integrated cross section for $E1$ photoabsorption in $^{56}$Ni, but makes a significant difference of $\bar{E}$, $\Gamma$, $\sigma_{max}$, and $\sigma_{-1}$ from the values calculated neglecting these correlations. This should also occur for the other nuclei studied.

•As expected, the influence of the one-particle continuum on the resonance shape and integrated characteristics is most important for light nuclei, especially for $^{48}$Ca. However, even for $^{208}$Pb this effect is not small. Inclusion of the continuum leads to an 8% increase of the resonance width $\Gamma$ and the integrated photoabsorption cross section $\sigma_0$, bringing themn close to the experimental values.

•The most important result is the satisfactory description of the total resonance widths $\Gamma$. The TOGD calculations underestimate $\Gamma$ by only 14%, 11.7%, and 4.4% for $^{40,48}$Ca and $^{208}$Pb, respectively.

•On the whole, the integrated characteristics of the $E1$ resonance, including the average energy $\bar{E}$, predicted for the radioactive nucleus $^{56}$Ni satisfy the known systematics of these parameters for stable nuclei.[54]

We see from Table II that the results of the RPA and TOGD calculations for the isovector $E2$ resonance in $^{40}$Ca and $^{208}$Pb are quite close and in fairly good agreement with the available experimental data. This is true particularly of the total resonance width and the cross section at the maximum $\sigma_0$ for $^{208}$Pb. However, if we take as a guide the experimental data for $^{208}$Pb from Ref. 56, which were obtained using highly polarized tagged photons and are probably the most accurate of all the experimental data presented in Table II, our calculations overestimate the average resonance energy by 2 MeV. We note that this energy can be made to agree with experiment by only slightly decreasing [by about 7% compared to that given in Eq. (78)] the isovector $f'$ amplitude of the effective $p-h$ interaction.

*Isoscalar $E2$ and $E0$ resonances in* $^{40}$Ca, $^{56}$Ni, *and* $^{208}$Pb nuclei. Study of the properties of isoscalar $E0$ resonances is particularly interesting, because it allows information to be obtained about the compression modulus of finite nuclei and nuclear matter, knowledge of which is important both for heavy-ion physics, and for astrophysics.[59]

The experimental data on this resonance are often very fragmentary and uncertain, particularly for nuclei with atomic weights $A<100$ (Ref. 59). Individual $E0$ structures characterized by relatively large total values of the percent saturation of the energy-weighted sum rules (EWSR) have been established for only a few of them. As a result, it is practically impossible to find the values of the compression modulus from these data, because they are directly determined in terms of the average resonance energy. One of the main reasons for the uncertainties in the experimental data is the difficulty of multipole decomposition of the various segments of the experimental spectra. As a rule, the same phenomenological collective form factors[59,60] are used for this, which do not include possible special features corresponding to individual fragments of the GMR. It thus becomes particularly important to perform a systematic microscopic analysis of the experimental data using approaches which take into account these special features.

Our calculations of the $E0$ resonance for $^{40}$Ca, $^{56}$Ni, and $^{208}$Pb (Refs. 31 and 32) have revealed an important feature which is common to all these nuclei: a strong effect of the GSC2 on the fragmentation of the $E0$ resonance, which produces low-energy ($E<10$ MeV) structures. The effect is strongest for $^{40}$Ca. The available experimental data for $^{40}$Ca and $^{208}$Pb (Refs. 61 and 62) confirm the presence of a large number of low-lying $E0$ states, but do not give their intensities. The values of the resonance width calculated for $^{208}$Pb, $\Gamma=2.3$ MeV and 56.4% of the EWSR($E0$) at energies $E=(11.6-16.4)$ MeV, are in fairly good agreement with experiment: $\Gamma=(2.4\pm0.3)$ MeV and $(47\pm19)$% of the EWSR($E0$) (Refs. 63 and 64).

The study of the effect of GSC2 on the properties of the $E2$ and $E0$ resonances in $^{40}$Ca was continued in Ref. 33. It was necessary to consider these resonances together because

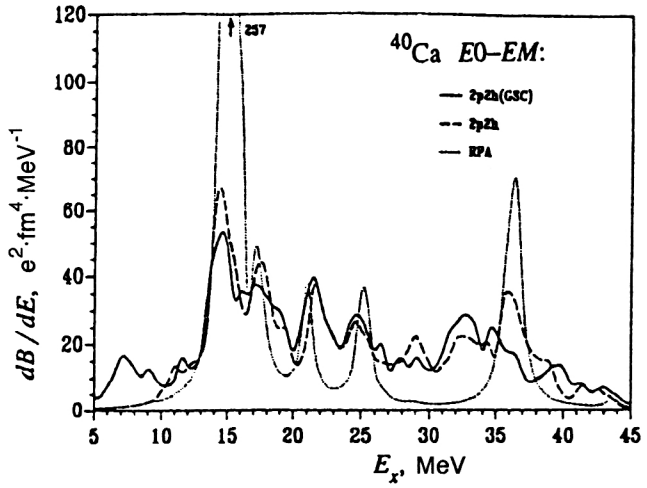


FIG. 9. Strength function of $E0$ excitations for electron scattering on $^{40}$Ca. The dotted line is the RPA calculation. The dashed and solid lines are the TOGD calculations respectively neglecting and including GSC2 effects. The continuum is included in all the calculations.

this study analyzed the results of an $(e,e')$ experiment[65] in which the contributions of the $E2$ and $E0$ multipoles to the observed cross sections are not distinguishable in principle. For comparison with experiment, the total $E2+E0$ strength function was calculated using the expression

$$\frac{dB(E2+E0)}{dE}=\frac{dB(E2)}{dE}+\frac{25}{16\pi}\frac{dB(E0)}{dE}. \tag{83}$$

The main results of the calculations are shown in Figs. 9–11 and in Table III, where predictions are also given for $^{56}$Ni. The percent saturation of the electromagnetic EWSR in various energy ranges given in the table were calculated using the expressions[60]

$$EWSR_{EM}(E0)=\frac{2\hbar^2}{m_p}Z\langle r^2\rangle_p,$$

$$EWSR_{EM}(E2)=\frac{50\hbar^2}{8\pi m_p}Z\langle r^2\rangle_p.$$

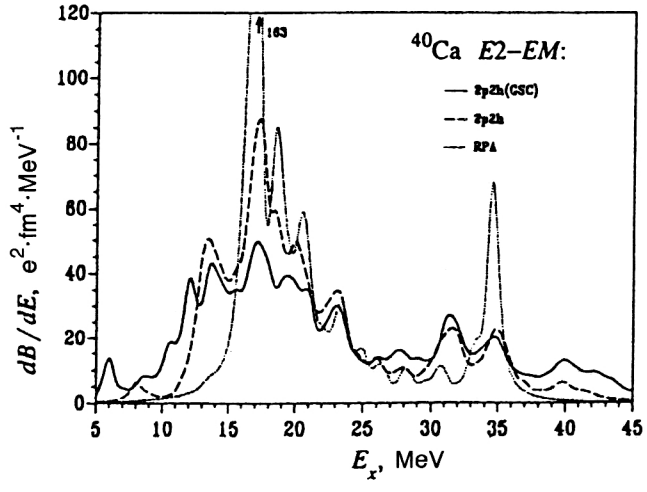


FIG. 10. The same as in Fig. 9, but for $E0$ excitations in $^{40}$Ca.

From our analysis of these results we arrive at the following conclusions:

•The RPA calculations of the $E2$ and $E0$ resonances do not describe the experimentally observed strong fragmentation of the total strength of $E2+E0$ excitations at energies $E=(10-20.5)$ MeV. The TOGD calculations neglecting GSC2 improve the agreement with experiment, but only the inclusion of these correlations allows a good description of both the energy of the main fragments of the strength function—12, 14, and 17 MeV, and also the corresponding absolute values of the transition strengths. The calculated value of the saturation $\mathrm{EWSR}_{EM}(E2+E0)=8436\,e^2\mathrm{F}^4$ MeV on this interval (23% of this comes from the $E0$ resonance) is in good agreement with the experimental value $(7899\pm1580)e^2\cdot\mathrm{fm}^4\cdot$MeV.

•Complete saturation of the $E2$ and $E0$ EWSR is attained only in a large energy range $E=(5-45)$ MeV, and the inclusion of GSC2 tends to increase the EWSR by 5% on the average compared to the RPA and TOGD calculations, in which these correlations are neglected. However, in the experimentally studied range the EWSR saturation is only 23% and 40% for the $E0$ and $E2$ resonances, respectively. Therefore, the main resonance strength is concentrated at energies $E>20.5$ MeV. It should be recalled that the results presented in Table III pertain to the total electromagnetic strength of the resonances. For their isoscalar components the saturation of the IS-EWSR$_{EM}$ is different: 50% and 60%. The total value calculated using an expression similar to Eq. (83), IS-EWSR$_{EM}(E2+E0)=85\%$, is in good agreement with experiment,[65] where the value $(80\pm16)\%$ was obtained. We also note that the calculated value of IS-EWSR$_{EM}(E0)=23\%$ in the range $E=(10.5-15.7)$ MeV is in very good agreement with the value $(23\pm5)\%$ obtained from analysis of the $(\alpha,\alpha')$ experiment.[63]

•Although it has some special features, the effect of GSC2 on resonance fragmentation in $^{56}$Ni is just as strong as for $^{40}$Ca.

*The $M1$ resonance in* $^{208}$Pb, $^{56}$Ni, *and* $^{100}$Sn. The neutron and proton subsystems of these nuclei each contain a pair of spin–orbit partners forming the $1p1h$ basis for the formation in the RPA of the isoscalar (IS) and isovector (IV) parts of the $M1$ resonance, which are split in energy by 2–3 MeV (see Figs. 12–14). The average energies of these resonances, given in Table IV, were calculated from the expression

$$\bar{E}=\frac{\Sigma_i E_i B_i(M1)}{\Sigma_i B_i(M1)}. \tag{84}$$

In turn, the total transition probabilities for the IS and IV $M1$ resonances were found by integrating the strength functions over the corresponding energy ranges. The parametrization of the local magnetic charge known from the theory of finite Fermi systems[35] was used in the calculation.

The results shown in Figs. 12–14 and Table IV suggest the following conclusions:

•The RPA and TOGD calculations are in fairly good agreement with each other in describing the average resonance energies $\bar{E}_{\mathrm{IS}}$ and $\bar{E}_{\mathrm{IV}}$ and the total probabilities

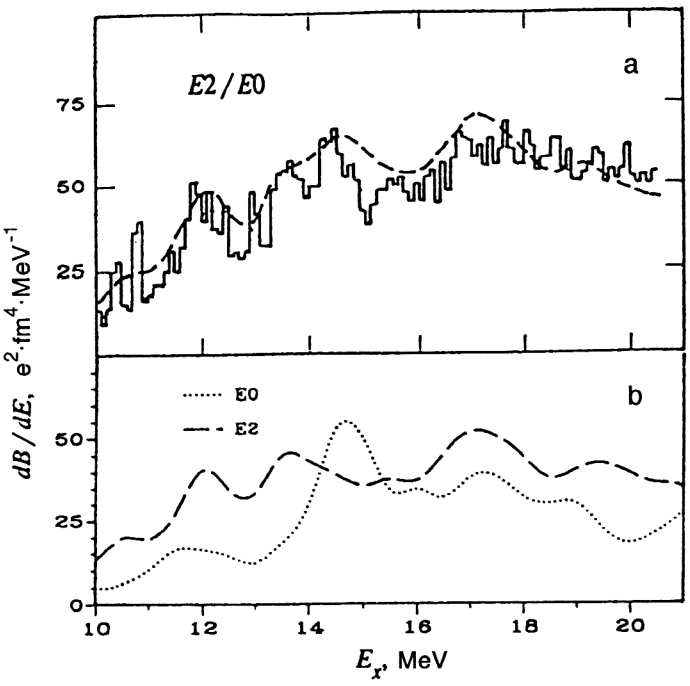


FIG. 11. (a) Total ($E2+E0$) strength function for electron scattering on $^{40}$Ca calculated using the TOGD method taking into account the continuum and GSC2 effects (dashed line); the histogram shows the experimental data from Ref. 65. The theoretical curve was obtained using (80). (b) Theoretical $E2$ (dashed line) and $E0$ (dotted line) components of the total strength function shown in Fig. 11a.

$\Sigma B(M1)$. However, the inclusion of complex $1p1h\otimes$phonon configurations in the calculation leads to significant suppression of the strength of the $M1$-IV resonance compared to the RPA and to the splitting off of a large fraction of $\Sigma B(M1)$ at energies $E>\bar{E}_{IV}$. The inclusion of GSC2 is manifested in additional redistribution of the total $M1$-transition probability.

•The total width of the IV$M1$ resonance in $^{208}$Pb obtained in the TOGD calculations ($\Gamma=1$ MeV) agrees with experiment, but the probability $B(M1)-IV=11.57\mu02$ is 25% smaller than the experimental value. On the other hand, the average resonance energy turned out to be 400 keV higher than the experimental value. The use of the effective interaction including $\pi$-meson exchange[35] in the calculations probably leads to a better description of the experimental data. Experimental studies of $M1$ excitations at energies $E>8.4$ MeV are of great interest; the calculations suggest that they account for 45% of $\Sigma B(M1)$.

•As seen from Figs. 12–14, the largest effect of fragmentation of the $M1$-IV resonance associated with the inclusion of complex configurations is obtained for $^{208}$Pb and $^{100}$Sn. Just as for $^{48}$Ca (Ref. 30), in $^{56}$Ni this resonance is scarcely fragmented. Owing to specific features of the one-particle proton spectrum (the binding energy $B_p=2.9$ MeV), both the isovector and the isoscalar components of the resonance are strongly split in the neutron-deficient nucleus $^{100}$Sn.

TABLE III. Saturation of the $EWSR_{EM}$ (in % of the $EWSR_{EM}$ values in $e^2\cdot fm^4\cdot MeV$) from the RPA and TOGD calculations including the continuum.

| | | | | |
|---|---|---|---|---|
| | $^{40}$Ca, $E0$, $EWSR_{EM}=16500$ | | | |
| $E_{min}-E_{max}$, MeV | 10–16 | 10–20.5 | 5–30 | 5–45 |
| RPA | 34.1 | 49.1 | 66.6 | 100.9 |
| TOGD | 14.3 | 29.0 | 55.3 | 101.6 |
| TOGD(GSC2) | 12.0 | 22.6 | 52.5 | 106.2 |
| | $^{40}$Ca, $E2$, $EWSR_{EM}=16412$ | | | |
| RPA | 4.5 | 45.5 | 72.0 | 101.0 |
| TOGD | 13.6 | 43.3 | 71.0 | 100.9 |
| TOGD(GSC2) | 17.2 | 40.1 | 64.6 | 105.8 |
| | $^{56}$Ni, $E0$, $EWSR_{EM}=31682$ | | | |
| RPA | 4.2 | 33.2 | 54.2 | 101.1 |
| TOGD | 4.3 | 28.3 | 52.0 | 101.4 |
| TOGD(GSC2) | 7.0 | 30.4 | 58.8 | 106.2 |
| | $^{56}$Ni, $E2$, $EWSR_{EM}=31514$ | | | |
| RPA | 14.2 | 33.7 | 70.4 | 99.5 |
| TOGD | 12.5 | 28.8 | 63.5 | 100.2 |
| TOGD(GSC2) | 12.0 | 29.5 | 62.0 | 104.6 |

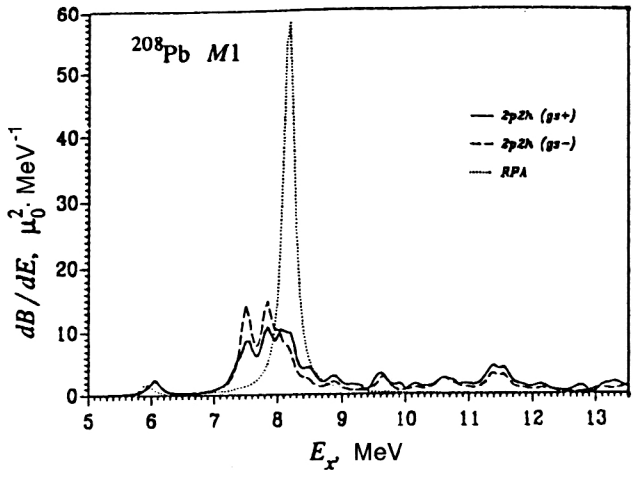


FIG. 12. Strength function of $M1$ excitations in $^{208}$Pb. The dotted line shows the RPA calculation, and the dashed and solid lines show the TOGD calculations respectively neglecting and including GSC2 effects. The continuum is included in all the calculations.

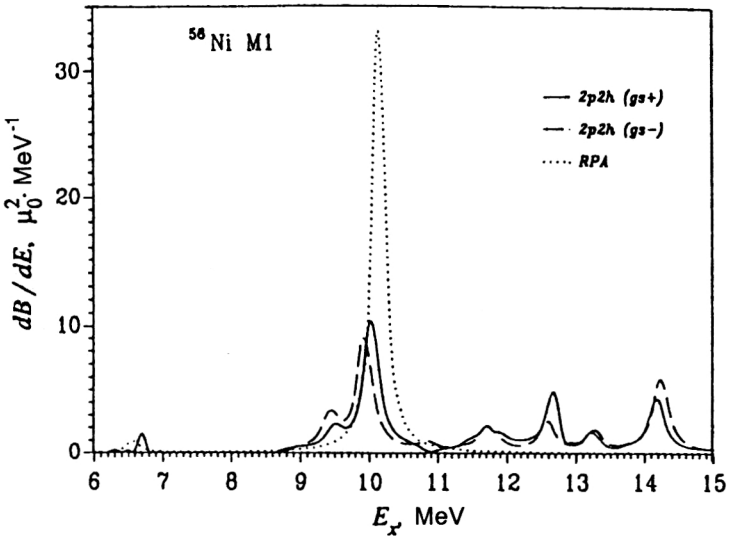


FIG. 13. The same as in Fig. 12, but for $^{56}$Ni.

## VII. CONCLUSIONS

In this review we have described a microscopic approach for analyzing the excited states of magic nuclei up to excitation energies of 30–40 MeV which is primarily applicable for giant-resonance calculations. Compared to the RPA, this approach includes the following additional contributions: (1) the one-particle continuum; (2) configurations of the type $1p1h\otimes$phonon; (3) ground-state correlations arising from these configurations. The theory has been realized numerically for GMRs in stable and unstable doubly magic nuclei using the nonseparable Landau–Migdal interaction.

In all the calculations we obtained reasonable agreement with the experimental data for the integrated characteristics of GMRs, including the total resonance widths. The fine structure of the isoscalar $E2$ resonance in $^{208}$Pb (Ref. 31) and the gross structure of the $E2$ and $E0$ resonances observed in reactions on $^{40}$Ca at excitation energies of 10–20 MeV (Ref. 33) are explained fairly well. In most cases, the inclusion of complex configurations significantly changes the results compared to the RPA; as a rule, it improves the agreement with experiment. This is also true for the continuum contribution.

The approach we have developed includes the ground-state correlations due to $1p1h\otimes$phonon configurations fairly systematically. It has been shown that these correlations must be included in describing the experimental data, as sometimes they are decisive in explaining an observed effect.

The success attained using this approach, which includes all three known mechanisms of GMR formation, allows us to anticipate that approaches of this type will also be able to explain low-lying resonance-like structures in the cross sections (this has been discussed earlier within the context of the quasiparticle–phonon model[20]), the numerous results of coincidence experiments, and, possibly, the fine structure of GMRs. At present these seem to be the most important questions in the physics of GMRs for cold nuclei. Unfortunately, the development of theory in this area significantly lags experiment. Natural directions for improvement and extension

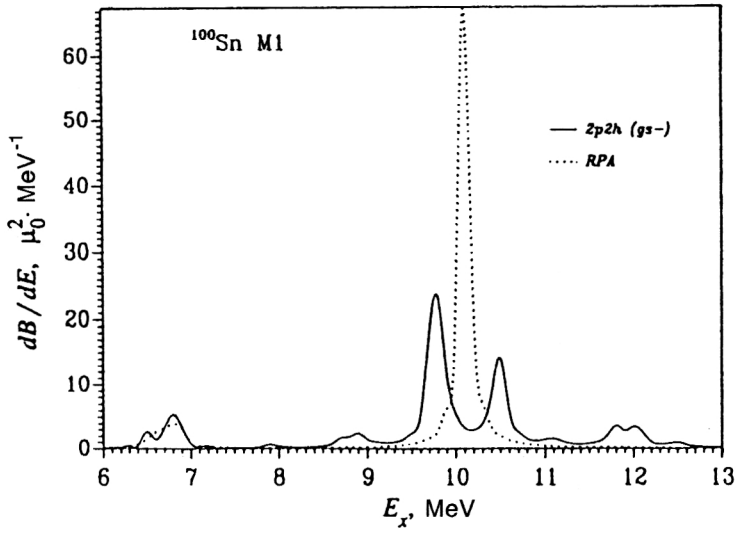


FIG. 14. The same as in Fig. 12, but for $^{100}$Sn. The TOGD calculations were performed neglecting GSC2 effects.

TABLE IV. Integrated characteristics of the $M1$ resonance from the RPA and TOGD calculations taking into account the continuum. GSC2 effects are not included in the calculations for $^{100}$Sn. $\bar{E}_{IS}$ and $\bar{E}_{IV}$ are given in MeV, and $B(M1)$−IS, $B(M1)$−IV, and $\Sigma B(M1)$ are given in $\mu_0^2$.

| | $\bar{E}_{IS}$, MeV | $B(M1)$−IS, $\mu_0^2$ | $\bar{E}_{IV}$, MeV | $B(M1)$−IV, $\mu_0^2$ | $\Sigma B(M1)$, $\mu_0^2$ |
|---|---|---|---|---|---|
| | | $^{208}$Pb (5–15.5)[a] | | | |
| RPA | 5.63 | 0.49 | 7.97 | 18.16 | 19.96 |
| TOGD | 5.72 | 0.84 | 7.66 | 11.87 | 19.09 |
| TOGD(GSC2) | 5.72 | 0.84 | 7.74 | 11.57 | 22.60 |
| Experiment | 5.85 | $1.9^{+0.7}_{-0.4}$ | 7.30 | 15.60 | |
| (Ref. 66) | 6.24 | | | (6.7–8.4)[b] | |
| | | $^{56}$Ni (5.5–15) | | | |
| RPA | 6.56 | 0.31 | 10.12 | 11.31 | 11.43 |
| TOGD | 6.70 | 0.24 | 9.93 | 4.80 | 10.62 |
| TOGD(GSC2) | 6.70 | 0.24 | 10.02 | 5.50 | 11.68 |
| | | $^{100}$Sn (6.0–13) | | | |
| RPA | 6.80 | 1.50 | 10.15 | 14.10 | 15.60 |
| TOGD[c] | 6.50 | 0.30 | 9.77 | 6.60 | |
| | 6.78 | 1.40 | 10.50 | 3.20 | 15.80 |

[a]$(E_{min}-E_{max})$ is the range for which the total transition probability $B(M1)$ is calculated.

[b]The experimental energy range corresponding to $\Sigma B(M1)_{ex}$.

[c]The two lines of the TOGD calculation refer to resonance fragments (see the text).

of the approach presented here are the following:

1. More careful analysis of the effects mimicked by the averaging parameter, because it turns out in practice that the TOGD method, like most other versions of the microscopic approach, explains the total observed resonance width only when this parameter is used.

2. Inclusion of consistency between the mean-field potential and the effective particle–hole interaction. At the present time there is no systematic, self-consistent approach taking into account complex configurations. The known methods of ensuring consistency actually work only within the RPA.

3. Generalization of our approach to nonmagic nuclei.

4. More detailed study of the effects of ground-state correlations due to complex configurations.

The authors are grateful to E. V. Litvinova for great help in preparing the figures.

This study was carried out with the partial support of the Russian Fund for Fundamental Research, grant No. 96-02-17250.

[1)]I.e., excitation energies of up to 30–40 MeV.

[2)]Here and below, the Fourier transforms of quantities depending on time differences will be defined as in Ref. 15. The numerical indices include the quantum numbers determining the one-particle functions of some complete basis set which will be specified later.

[3)]The rearranged perturbation theory can be formulated more rigorously, but the detailed discussion of this lies outside the scope of this study.

[4)]The approximate equality $\sim$ of these quantities is introduced in order to distinguish them from the analogous quantities $e_q$ and $\mathscr{F}$ defined in the theory of finite Fermi systems.

[5)]For simplicity, we shall sometimes use the term $2p2h$ configuration for both "pure" $2p2h$ configurations and $1p1h\otimes$phonon configurations, because in the RPA the phonon is a superposition of $1p1h$ configurations.

[6)]See, for example, the general expressions for $A(\mathbf{r},\mathbf{r}_1;\omega)$ in the $g^2$ approximation obtained in Ref. 46.

[7)]Separately for each partial $l,j$ component; the other potential parameters are set equal to the empirical values.[48]

[1] *Electric and Magnetic Giant Resonances in Nuclei*, edited by J. Speth (World Scientific, Singapore, 1991).
[2] S. Drożdż, S. Nishizaki, J. Speth, and J. Wambach, Phys. Rep. **197**, 1 (1990).
[3] S. P. Kamerdzhiev, in *Proc. of the Fourth Seminar on Electromagnetic Interactions of Nuclei at Low and Intermediate Energies* [in Russian] (Nauka, Moscow, 1979), p. 93.
[4] É. E. Sapershteĭn, S. A. Fayans, and V. A. Khodel', Preprint IAÉ-2580 (1976) [in Russian].
[5] S. Shlomo and G. Bertsch, Nucl. Phys. **A243**, 507 (1975).
[6] M. Buballa, A. Gattone, R. De Haro *et al.*, Nucl. Phys. **A517**, 61 (1990).
[7] Nguyen Van Giai, P. F. Bortignon, A. Bracco, and R. A. Broglia, Phys. Lett. **233B**, 1 (1989); Nguyen Van Giai and Ch. Stoyanov, Phys. Lett. **252B**, 9 (1990).
[8] V. G. Soloviev (Solov'ev), *Theory of Complex Nuclei* (Pergamon Press, Oxford, 1976) [Russ. original, Nauka, Moscow, 1971].
[9] J. Sawicki, Phys. Rev. **126**, 2231 (1962).
[10] K. Takayanagi, K. Shimizu, and A. Arima, Nucl. Phys. **A477**, 205 (1988); **A481**, 313 (1988).
[11] S. Adachi and E. Lipparini, Nucl. Phys. **A489**, 445 (1988).
[12] G. F. Bertsch, P. F. Bortignon, R. A. Broglia, and C. H. Dasso, Phys. Lett. **80B**, 161 (1979).
[13] P. F. Bortignon and R. A. Broglia, Nucl. Phys. **A371**, 405 (1981).
[14] S. P. Kamerdzhiev, JETP Lett. **30**, 500 (1979); Yad. Fiz. **38**, 316 (1983) [Sov. J. Nucl. Phys. **38**, 188 (1983)].
[15] S. P. Kamerdzhiev and V. I. Tselyaev, Yad. Fiz. **44**, 336 (1986) [Sov. J. Nucl. Phys. **44**, 214 (1986)].
[16] S. P. Kamerdzhiev and V. N. Tkachev, Z. Phys. A **334**, 19 (1989).
[17] S. P. Kamerdzhiev, J. Speth, G. Tertychny, and V. Tselyaev, Nucl. Phys. **A555**, 90 (1993).
[18] V. I. Tselyaev, Yad. Fiz. **50**, 1252 (1989) [Sov. J. Nucl. Phys. **50**, 780 (1989)].
[19] R. A. Eramzhyan, B. S. Ishkhanov, I. M. Kapitonov, and V. G. Neudachin, Phys. Rep. **136**, 229 (1986).
[20] S. N. Belyaev, O. V. Vasil'ev, V. V. Voronov *et al.*, Yad. Fiz. **55**, 289 (1992) [Sov. J. Nucl. Phys. **55**, 157 (1992)]; Fiz. Élem. Chastits At. Yadra **23**, 1537 (1992) [Sov. J. Part. Nucl. **23**, 667 (1992)].
[21] B. Dolbilkin, Izv. Akad. Nauk SSSR, Ser. Fiz. **55**, 967 (1991).
[22] M. A. Hofstee, S. Y. van der Werf *et al.*, Nucl. Phys. **A588**, 729 (1995).
[23] S. Adachi and S. Yoshida, Nucl. Phys. **A462**, 61 (1987).
[24] E. Migli, S. Drożdż, J. Speth, and J. Wambach, Z. Phys. A **340**, 111 (1991).
[25] G. Colo, P. F. Bortignon, Nguyen Van Giai *et al.*, Phys. Lett. **276B**, 279 (1992).
[26] G. Colo, N. Van Giai, P. F. Bortignon *et al.*, Phys. Rev. C **50**, 1496 (1994).
[27] S. P. Kamerdzhiev and G. Ya. Tertychnyĭ, JETP Lett. **53**, 412 (1991).
[28] S. Kamerdzhiev, G. Tertychny, and W. Unkelbach, Phys. Lett. **287B**, 293 (1992).
[29] S. Kamerdzhiev, J. Speth, and G. Tertychny, in *Variations on Nuclear Themes*, edited by C. M. Class and L. Cohen (World Scientific, Singapore, 1994), p. 103.
[30] S. Kamerdzhiev, J. Speth, G. Tertychny, and J. Wambach, Z. Phys. A **346**, 253 (1993).
[31] S. Kamerdzhiev, G. Tertychny, and J. Speth, Nucl. Phys. **A569**, 313c (1994).
[32] S. Kamerdzhiev, G. Tertychny, J. Speth, and J. Wambach, Nucl. Phys. **A577**, 641 (1994).
[33] S. Kamerdzhiev, J. Speth, and G. Tertychny, Phys. Rev. Lett. **74**, 3943 (1995).
[34] S. Kamerdzhiev and J. Speth, Nucl. Phys. **A599**, 373c (1996).
[35] A. B. Migdal, *Theory of Finite Fermi Systems and Applications to Atomic Nuclei*, transl. of 1st Russ. ed. (Interscience, New York, 1967) [Russ. original, Nauka, Moscow, 1983].
[36] S. P. Kamerdzhiev and V. I. Tselyaev, Izv. Akad. Nauk SSSR, Ser. Fiz. **55**, 49 (1991).
[37] V. I. Tselyaev, Izv. Akad. Nauk SSSR, Ser. Fiz. **57**, No. 10, 34 (1993)
[38] S. Ethofer, Z. Phys. **255**, 353 (1969).
[39] J. Speth, E. Werner, and W. Wild, Phys. Rep. **33**, 127 (1977).
[40] P. F. Bortignon, R. A. Broglia, D. R. Bes, and R. Liotta, Phys. Rep. **30**, 305 (1977).

[41] V. G. Solov'ev, *Theory of the Nucleus. Quasiparticles and Phonons* (Institute of Physics, Bristol, 1992) [Russ. original, Énergoatomizdat, Moscow, 1989].
[42] V. S. Vladimirov, *Equations of Mathematical Physics* (Dekker, New York, 1971) [Russ. original, Nauka, Moscow, 1981].
[43] A. Bohr and B. R. Mottelson, *Nuclear Structure*, Vol. 2 (Benjamin, New York, 1975) [Russ. transl., Mir, Moscow, 1977].
[44] V. Paar, Phys. Lett. **B60**, 232 (1976).
[45] D. Karadjov, V. V. Voronov, and F. Catara, Phys. Lett. **B306**, 197 (1993).
[46] S. P. Kamerdzhiev and V. N. Tkachev, Yad. Fiz. **43**, 1426 (1986) [Sov. J. Nucl. Phys. **43**, 918 (1986)].
[47] A. P. Platonov and É. E. Sapershteĭn, Yad. Fiz. **46**, 437 (1987) [Sov. J. Nucl. Phys. **46**, 231 (1987)].
[48] V. A. Chepurnov, Yad. Fiz. **6**, 955 (1967) [Sov. J. Nucl. Phys. **6**, 696 (1967)].
[49] A. V. Smirnov, S. V. Tolokonnikov, R. F. Fayazov, and S. A. Fayans, Preprint IAÉ-4281/2 (1986) [in Russian]; Yad. Fiz. **48**, 1661 (1988) [Sov. J. Nucl. Phys. **48**, 995 (1988)].
[50] I. N. Borzov, S. V. Tolokonnikov, and S. A. Fayans, Yad. Fiz. **40**, 1151 (1984) [Sov. J. Nucl. Phys. **40**, 732 (1984)].
[51] J. Ahrens, H. Borchert, K. H. Czock *et al.*, Nucl. Phys. **A251**, 479 (1975).
[52] G. J. O'Keefe, M. N. Thompson, Y. I. Assafiri *et al.*, Nucl. Phys. **A469**, 239 (1987).
[53] A. Veyssiere, H. Beil, R. Bergere *et al.*, Nucl. Phys. **A159**, 561 (1970).
[54] B. L. Berman and S. C. Fultz, Rev. Mod. Phys. **47**, 713 (1975).
[55] I. Bergqvist, R. Zorro, A. Hakansson *et al.*, Nucl. Phys. **A419**, 509 (1984).
[56] D. S. Dale, R. M. Laszewski, and R. Alarcon, Phys. Rev. Lett. **68**, 3507 (1992).
[57] F. E. Bertrand and J. R. Beene, in *Proc. of the 1989 Intern. Nuclear Physics Conf.*, edited by M. S. Hussein (World Scientific, Singapore, 1990), Vol. 2, p. 397.
[58] T. Murakami, I. Halpern, D. W. Storm *et al.*, Phys. Rev. C **35**, 479 (1987).
[59] A. Van der Woude, in *Electric and Magnetic Giant Resonances in Nuclei*, edited by J. Speth (World Scientific, Singapore, 1991), p. 99.
[60] G. R. Satchler, *Direct Nuclear Reactions* (Clarendon Press, Oxford, 1983).
[61] P. M. Endt, Nucl. Phys. **A521**, 624 (1990).
[62] M. J. Martin, Nucl. Data Sheets **47**, 797 (1986).
[63] S. Brandenburg, W. T. A. Borghols, A. G. Drentje *et al.*, Nucl. Phys. **A466**, 29 (1987).
[64] T. Yamagata, S. Kishimoto, K. Yuasa *et al.*, Nucl. Phys. **A381**, 277 (1982).
[65] H. Diesener, U. Helm, G. Herbert *et al.*, Phys. Rev. Lett. **72**, 1994 (1994); P. von Neumann-Cosel, in *Proc. of the Fourth Intern. Conf. on Selected Topics in Nuclear Structure*, Dubna, Russia, 1994.
[66] R. M. Laszewski, R. Alarcon, D. S. Dale, and S. D. Hoblit, Phys. Rev. Lett. **61**, 1710 (1988).

Translated by Patricia A. Millard